

MSE307 Units 2A and 2B

Units 2A and 2B serve, mostly as revision based on your lectures in MSE203 and MSE204, to remind you of how we manipulate phase transformations and microstructure (normally using thermomechanical processing) to design in the mechanical properties that we require of a particular steel. So we look first at the principal means of achieving strength and toughness, then at the phase transformations and microstructures that are typical for steel. If you'd like right from the beginning to take home a *leitmotif* of Units 2 and 6 then it is the **transformation from austenite to ferrite in steel**.

1 Strength, toughness and ductility

The purpose of the first part of this unit is to remind you of the various measurable mechanical properties of metal alloys and to provide you with a brief analysis of these in the case of steels.

You are aware of the notions of ductility, strength and toughness. Ductility is usually expressed in terms of elongation or reduction in area. Strength may be specified as yield strength, proof stress or (ultimate) tensile strength. Toughness is strictly a measure of critical stress intensity, or fracture toughness; but is also commonly assessed as energy absorbed (in a Charpy test) or impact transition temperature (ITT) in the case that the metal exhibits a ductile to brittle transition.

Slides 1–14 are to remind you of the principal strengthening mechanism available to the materials designer. They are, solid solution, particle, grain boundary and transformation strengthening.

Slides 2 and 3 emphasise the usual linear dependence of yield stress on alloying element composition, and the particularly large effect that interstitials have compared to substitutional elements. **Slide 3** shows the rough correlation between size misfit and strengthening coefficient.

The theories of particle and grain boundary strengthening are summarised. **Slides 10 and 11** remind us, here in the context of a low carbon steel, that alone among these mechanisms grain refinement will improve both strength and toughness. This is the exception to the rule that greater strength in general is associated with a lesser toughness in metals.

There are at least four ways to ‘derive’ the Hall–Petch equation. A simple one due to Cottrell is to use the similarity of the stress due to a pile up of dislocations on a slip plane under an applied shear stress τ_s , and the stress due to a shear crack. The crack tip stress takes the form

$$\tau(r) \approx (\tau_s - \tau_i) \sqrt{\frac{d}{r}}$$

at a distance r from its tip, if d is the length of the slip plane and τ_i is the friction stress.

The assumption is that yielding will occur when the stress at a distance r_c ahead of the tip of the pile up reaches a critical value τ_c . This leads us to a yield stress,

$$\tau_y = \tau_i + k_y d^{-\frac{1}{2}}$$

which is the Hall–Petch equation with $k_y = \tau_c r_c$.

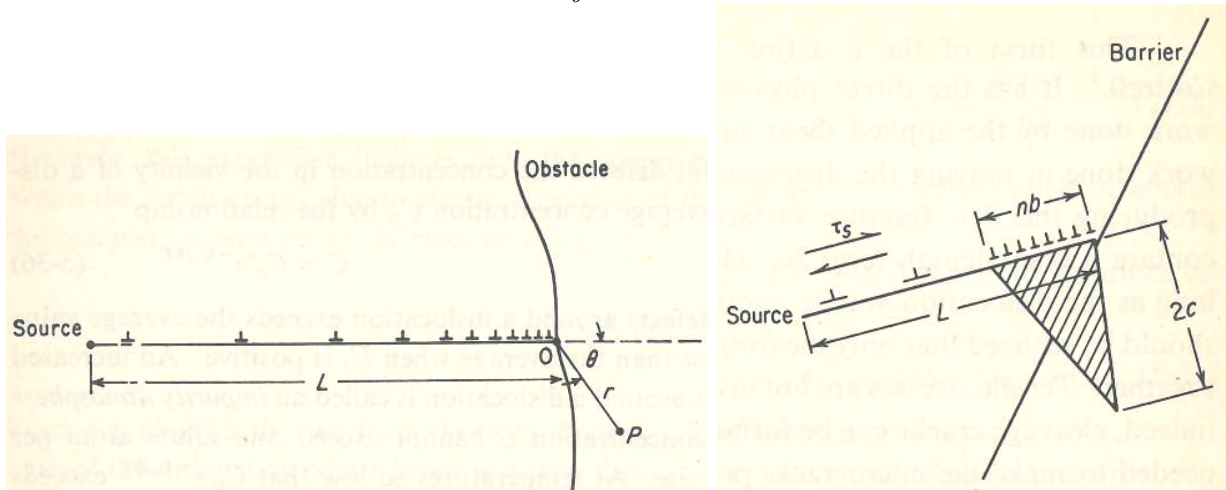


Figure 1

Consider figure 1. The normal stress acting across OP is

$$\sigma = \frac{3}{2} \sqrt{\frac{L}{r}} \tau_s \cos \frac{1}{2} \theta \sin \theta$$

and the maximum value of this is

$$\sigma_{\max} = \frac{3}{2} \sqrt{\frac{L}{r}} \tau_s$$

The shear stress acting in the plane OP is (see Dieter, equation 5.41)

$$\tau \approx \tau_s \sqrt{\frac{L}{r}}$$

If we account also for the friction stress, τ_i , then we need to replace τ_s with $\tau_s - \tau_i$ and equating the tensile stress at r with the cohesive strength we get

$$(\tau_s - \tau_i) \sqrt{\frac{L}{r}} = \sqrt{\frac{E\gamma_s}{a}}$$

where the right hand side is the Orowan cohesive strength with E , the Young's modulus, γ_s is the surface energy and a is the lattice constant. This implies that microcrack initiation occurs at an applied shear stress of

$$\tau_s = \tau_i + \sqrt{\frac{Er\gamma_s}{La}}$$

If we allow that $a \approx r$ and $E = 2\mu$ (twice the shear modulus) then

$$\tau_s = \tau_i + \sqrt{\frac{2\mu\gamma_s}{L}}$$

The number of dislocations, n , in the pile up is given by

$$nb \approx (\tau_s - \tau_i) \frac{L}{\mu} \quad (1)$$

where b is the Burgers vector, and eliminating L/μ , we get

$$(\tau_s - \tau_i) nb \approx 2\gamma_s \quad (2)$$

If I rearrange this into

$$\tau_s nb = \tau_i nb + 2\gamma_s$$

then, in words, this reads that the *work done by the applied stress in producing a displacement nb* is equal to the *work done in moving the n dislocations against the friction stress* plus the *energy to create two new surfaces*. This is a criterion for the nucleation of a microcrack. Its propagation is the result of a normal stress

$$\sigma = 2(\tau_s - \tau_i)$$

So we rewrite (2) as

$$\sigma nb = 4\gamma_s$$

and using (1) we get

$$\sigma (\tau_s - \tau_i) d = 8\mu\gamma_s$$

where we assert that $L = d/2$ if d is the grain diameter. If the microcracks form when $\tau_s = \tau_y$ the yield stress, then from the Hall-Petch equation,

$$\begin{aligned} \tau_s = \tau_y &= \frac{1}{2}\sigma_y \quad ; \quad \tau_i = \frac{1}{2}\sigma_i \\ \sigma_y &= \sigma_i + k_y d^{-\frac{1}{2}} \\ \tau_s - \tau_i &= 2k_y d^{-\frac{1}{2}} \end{aligned}$$

Then at fracture

$$\sigma = \sigma_f = \frac{4\mu\gamma_s}{k_y} d^{-\frac{1}{2}}$$

which is the Cottrell–Petch equation on **slide 9**.

2 Fe–C phase diagram

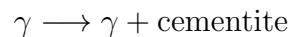
Steel is heat treatable because pure iron undergoes a phase transformation from body centred cubic (bcc) to face centred cubic (fcc) as it is heated through 912°C. This

transformation temperature depends on the carbon concentration as shown in the well-known iron–carbon phase diagram. I couldn't decide which of the many illustrated in textbooks and on-line to show you, so I have supplied you with a whole set of these in **slides 13–19** to study at home. You need to be familiar with the names given to the various phase boundary lines, such as A_1 , A_2 , and so on; and the subscripts “c” for heating and “r” for cooling. As you see in **slide 19** there is hysteresis: the A_3 phase boundary, for example, lies at a higher temperature for heating than for cooling—there will always be a certain amount of undercooling possible, depending on the rate of temperature change.

In cooling slowly from the austenite field, at not too low a temperature, the reactions depend on whether the nominal carbon concentration is below or above the eutectoid composition of about 0.8 wt%. In a hypoeutectoid steel the reaction is



with the γ becoming increasingly carbon rich until it reaches 0.8 wt%. Then pearlite forms. Conversely in a hypereutectoid steel the reaction is



with γ being increasingly carbon depleted until it reaches 0.8 wt%. Then pearlite forms.

3 Phase transformation

Reconstructive solid state phase transformations can only happen as a result of diffusing atoms. We will look at the theory of diffusion in Unit 2E; here I just show you some data to give you orders of magnitude feeling for the distances and times involved. **Slide 24** is taken from L. S. Darken and gives a very useful overview of this for both interstitial and substitutional diffusion in iron. One way to use this diagram is to follow the three columns on the right. The column headed “jump time” gives the reciprocal jumping frequency, (we'll call this ν in the Unit 2E notes) or mean residence time of an atom in between jumps. $\nu_0 = kT/h$ is the fundamental attempt frequency in statistical mechanics. For example for nitrogen in iron at 100°C read across to find that on average the N atom jumps about once every millisecond, whereas at that temperature a substitutional atom, say Cr, is essentially frozen in place. The two left hand columns are using the well known $d = \sqrt{Dt}$ to estimate the time taken for an atom to travel to a grain boundary or through a slab thickness. Again for N at 100°C the time needed to migrate across a 2mm slab is roughly the age of the Universe.

We need to be able to classify types of phase transformations in order to understand the underlying fundamental physics that controls the process. Remember that phase diagrams chart the equilibrium or possibly para-equilibrium (maybe even “near equilibrium”) distribution of crystal structure and compositions as functions of temperature and nominal alloy composition. The other side of the coin is the kinetics of phase transformations. These will be dominated by numerous factors, one of which is the diffusivity of alloying elements if the phases are to remain in equilibrium or para-equilibrium. **Slides 22–24** show some diffusivity data.

In the remainder of **units 2A** and **2B** we study phase transformations in steel.

Slide 26 shows a chart linking all the types of phase transformation in metals and alloys into a single classification.

Slide 27 shows a table listing the types of phase transformations and associated microstructures in steel.

Next, I remind you of the *TTT* diagram; followed by a discussion of the austenite to ferrite transformation. This latter topic is in effect the *leitmotif* of both **units 2** and **6** as I hope to make very clear.

Slides 32–47 if you've not seen this before are your first introduction to the products of decomposition of austenite to ferrite that are available to the ferrous alloy designer. The phases are classified (according to C. A. Dubé in 1948) into these categories:

1. Grain boundary allotriomorphs. Nucleate at g.b.'s at 800–850°C having curved boundaries. Equiaxed or lenticular; may develop facets at low temperature with respect to one grain: $\{111\}_\gamma || \{110\}_\alpha; \langle 110 \rangle_\gamma || \langle 111 \rangle_\alpha$
2. Widmanstätten side plates or laths. Nucleate at g.b.'s but grow along well defined planes of the austenite. May also nucleate at boundaries between pre-existing allotriomorphic ferrite and austenite.
3. Intragranular idiomorphs: roughly equiaxed; nucleate within the austenite grains.
4. Intragranular plates.

Slides 48–52 amount to an instructive case study showing how it is possible by heat treatment to design a microstructure having either acicular ferrite, bainite or martensite. This will be discussed in class and the original paper by Babu and Bhadeshia will be found on the Blackboard.

Further reading

G. E. Dieter, “Mechanical Metallurgy”, McGraw-Hill (any edition)

<http://www.tms.org/pubs/journals/jom/9801/felkins-9801.html>

R. W. K. Honeycombe, “Steels: Microstructure and Properties,” Edward Arnold, 1st Edition, 1981

H. K. D. H. Bhadeshia and R. W. K. Honeycombe, “Steels: Microstructure and Properties,” Elsevier, 3rd Edition, 2006

S. S. Babu and H. K. D. H. Bhadeshia, *Materials Trans. JIM*, **32** 679 (1991) [uploaded to the Blackboard.]

Problems

- 1 Give arguments for why *both* the yield and fracture strengths of steel should depend on the inverse square root of the grain size. See *The Mechanical Properties of Matter*, A. H. Cottrell, John Wiley, 1964.
- 2 Considering only the effects of grain size, impact transition temperature *decreases* linearly with the inverse square root of the mean grain size. Yield strength *increases* linearly with the inverse square root of the mean grain size. Use these two facts to show that the impact transition temperature *decreases* linearly with increasing yield strength.
- 3 In the tensile test a specimen having gauge length l_0 and cross-sectional area A_0 is pulled to a final length l_f by application of a force F . Define the true stress σ and true strain ε and the engineering stress s and engineering strain e in terms of these quantities. Given that volume is conserved during plastic deformation find a relation between e and ε and a relation between s and σ , and show that

$$\frac{de}{d\varepsilon} = 1 + e$$

and

$$\frac{ds}{d\sigma} = \exp(-\varepsilon) \left[1 - \sigma \frac{d\varepsilon}{d\sigma} \right]$$

Sketch a typical stress-strain curve in the tensile test, showing both s and σ as functions of the true strain. The true stress is a non decreasing function of ε whereas there is a maximum in the s - ε curve at the point of necking instability. This occurs at an engineering stress, s_u , called the *ultimate tensile strength*, U.T.S., or tensile strength for short. Since there is a maximum in the s - ε curve it is clear that the condition at U.T.S. is

$$\left(\frac{ds}{d\varepsilon} \right)_u = 0$$

Show that at U.T.S.

$$\left(\frac{d\sigma}{d\varepsilon} \right)_u = \sigma_u \tag{P1}$$

where σ_u is the true stress at necking. This expresses the condition that necking occurs at the point where the work hardening rate becomes smaller than the instantaneous true stress; illustrate this on your diagram. Show that

$$\left(\frac{d\sigma}{de} \right)_u = \frac{\sigma_u}{1 + e}$$

This is the basis for Considère's construction. Illustrate this by a plot of true stress against engineering strain in which a straight line that passes through $e = -1$ makes a tangent with the stress strain curve at σ_u .

Show that the equation (P1) holds for the special case of the Ludwik work hardening rule,

$$\sigma = \sigma_i + k\varepsilon^n$$

- 4 A thin walled tube is made from steel having a shear modulus of 80 GPa and a yield strength of 900 MPa. The radius of the tube is 100 mm, the length is 1 m and the wall thickness is 1 mm. A torque of 3000 Nm is applied to one end and the other end is clamped. Calculate the angle of twist.
- 5 A microalloy steel is strengthened with incoherent carbide precipitates. Their centre-to-centre separation is on average 6×10^{-8} m. Estimate the increase in yield strength due to the particles.
- 6 Can you think of a reason why carbon is fairly soluble in fcc iron but almost completely insoluble in bcc iron?
- 7 How can you deduce from the iron-carbon phase diagram that carbon is an austenite stabiliser?
- 8 Carbon is deposited on the surface of a piece of bcc iron which is held at 250°C. Estimate the time required for the carbon to diffuse 2 mm below the surface. Repeat the estimate for hydrogen instead of carbon.
- 9 What is meant by an *athermal* phase transformation?
- 10 Describe and contrast the microstructures of plate and lath martensite. Under what conditions of steel composition and heat treatment would you expect the two to appear? What is a “burst” in this context?
- 11 Use sketches of the microstructure to illustrate the various types of ferrite: grain boundary, idiomorphic, allotriomorphic, and Widmanstätten. Which of these grows by a *displacive mechanism*?

Lecture 3

It is of course of great importance to study the decomposition of austenite since it exactly this process which happens during the cooling of a steel. In fact this is the principal theme of most of these lectures.

Slides 2–8 are some remarkable time-lapse micrographs of the growths of the four principal austenite decomposition products, namely allotriomorphic and Widmanstätten ferrite, martensite and bainite. These were published by Marder (see further reading).

We use TTT diagrams to predict the mode of austenite decomposition and the transformation products to expect. **Slide 10** is a cartoon TTT diagram indicating the principal decomposition products of austenite. It is now generally accepted that there are separate bays or TTT curves for pearlite, upper and lower bainite.

Examples are shown in **slide 11**, taken from the paper by Irwin and Pickering that I mentioned in **lecture 2**. Note the effect of molybdenum and manganese is to move the bays to longer times and especially to delay the growth of pearlite. This is shown in the cartoon **slide 12**. Note that the growth of pearlite is *reconstructive* whereas the growth of bainite is *displacive* (see **slide 13**).

Firstly we will study the higher temperature heat treatments that result largely in reconstructive (or “civilian”) transformations. These are dominated by thermal activation and diffusion and the key feature of these is in the kinetics—*the amount transformed depends on time*, whereas the rate of transformation depends on temperature.

Slide 14 shows cartoons of the four most typical microstructures found in steels. The point of this lecture course is to teach you how to obtain and exploit these microstructures by alloying and by heat treatment so as to design steels of required mechanical properties. The top two, ferrite and pearlite, are reconstructive decomposition products and we discuss these first.

Slide 16 introduces you to the notion of extrapolating phase boundaries in the equilibrium diagram. The inverted triangle thus formed by broken lines below the eutectoid point encloses a region of temperature and composition within which a supercooled homogeneous alloy will be supersaturated with respect to both cementite (c) and ferrite (α). To the right is the corresponding TTT diagram for growth of pearlite. At the representative temperature indicated by a horizontal broken line in the phase diagram we are above the “nose” or “bay” of the pearlite TTT and pearlite growth will occur in a so called *discontinuous precipitation* as indicated in **slide 17**. The parameters from **slides 16** and **17** enter into the “Zener–Hillert” formula for the speed of growth, V , namely the velocity of the interface normal to itself. Actually the pearlite is growing into spherical nodules. The lamellar thickness λ is inversely proportional to the undercooling and so is fixed; it doesn’t appear so in **slides 16–18** of **Lecture 2** but this is because different pearlite nodules are sectioned at different angles.

The remaining slides concern the growth of proeutectoid ferrite, classified (according to C. A. Dubé in 1948) into these categories

1. Grain boundary allotriomorphs. Nucleate at g.b.'s at 800–850°C having curved boundaries. Equiaxed or lenticular; may develop facets at low temperature with respect to one grain: $\{111\}_\gamma || \{110\}_\alpha; \langle 110 \rangle_\gamma || \langle 111 \rangle_\alpha$
2. Widmanstätten side plates or laths. Nucleate at g.b.'s but grow along well defined planes of the austenite. May also nucleate at boundaries between pre-existing allotriomorphic ferrite and austenite.
3. Intragranular idiomorphs: roughly equiaxed; nucleate within the austenite grains.
4. Intragranular plates.

Further reading

J. W. Martin, R. D. Doherty and B. Cantor, “Stability of microstructure in metallic systems,” Cambridge University Press, 2nd edition, 1997

A. R. Marder, “Structure-property relationships in ferrous transformation products” in *Phase transformations in ferrous alloys*, Metall. Soc. AIME (1984) p. 11

B. L. Bramfitt and A. R. Marder, *Met. Trans.*, **4**, 2291 (1973)

R. W. K. Honeycombe, “Steels: Microstructure and Properties,” Edward Arnold, 1st Edition, 1981

https://www.youtube.com/watch?v=hXUmqM_8yJ4

Seung-Woo Seo, H. K. D. H. Bhadeshia and Dong Woo Suh, *Mat. Sci. Technol.*, **31**, 487 (2015)

Problems

- 3.1 Describe and contrast the microstructures of plate and lath martensite. Under what conditions of steel composition and heat treatment would you expect the two to appear? What is a “burst” in this context?
- 3.2 Use sketches of the microstructure to illustrate the various types of ferrite: grain boundary, idiomorphic, allotriomorphic, and Widmanstätten. Which of these grows by a *displacive mechanism*?

MSE307 Unit 2C

Unit 2C specifically concerns the *reconstructive* transformation from austenite (γ) to proeutectoid ferrite (α). This means that we are studying the isothermal (that is, a hold at constant temperature) transformation of a steel at a carbon (and possibly additional element) content and temperature that places the system in the two-phase $\alpha + \gamma$ region of the phase diagram that is bounded by A_1 , A_3 and the no-name line that is the limit of solubility of carbon in ferrite. Because this is a reconstructive transformation it is fully diffusion controlled and entails no shape change between parent and product phase. So by reference to **Slide 0** we are dealing principally with idiomorphic or allotriomorphic ferrite here. Actually for simplicity I will describe a one-dimensional model for the growth (even that is hard enough) so you may think of this as allotriomorphic ferrite which has initially spread rapidly along the austenite grain boundary since grain boundary growth is rapid, and then it sets out into the γ -grain: the planar boundary moving normal to itself (see **units 2A 2B, Slide 40**).

We focus therefore on the interface itself and ask how the *partitioning* of both carbon and substitutional elements across the interface, in an attempt to achieve equilibrium between the two phases, controls the rate of motion of the interface and hence the rate of the transformation from austenite to ferrite. The central assumption is that at all times, at the interface, there is *local equilibrium* of all the alloying elements. That is to say that if the interface is moving from left to right, say, then immediately to the left of the interface the composition is such that each component is in equilibrium with the ferrite, and immediately to the right each component is in equilibrium with the austenite. This requires that the interface compositions are dictated by tie lines in the phase diagram.

1. Binary Fe–C alloy

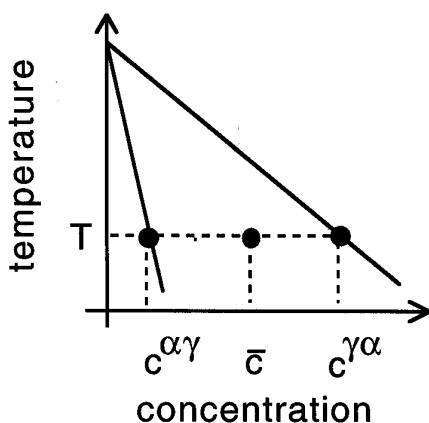


Figure 1

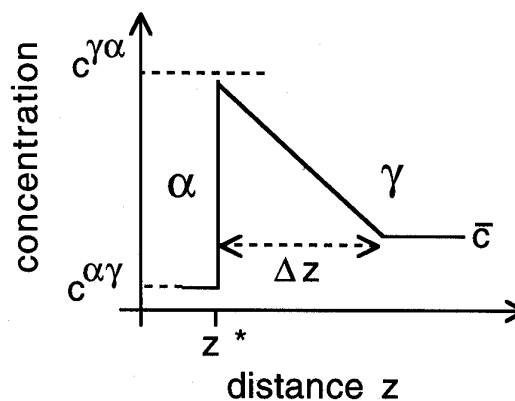


Figure 2

We use figures 1 and 2 to set the scene and to establish notation. At a temperature T and a concentration of carbon \bar{c} this places us in the two phase $\alpha + \gamma$ field of the Fe–C

phase diagram and figure 1 shows a tie line between A_3 and the no-name line. At the ends of the tie line are $c^{\alpha\gamma}$ which is the concentration of carbon in iron in the ferrite which is in equilibrium with carbon in the austenite, with $c^{\gamma\alpha}$ similarly defined. Figure 2 then shows a model concentration profile of carbon near the moving $\alpha-\gamma$ interface. The interface is currently at position z^* along the z -axis which we have set perpendicular to the moving planar $\alpha-\gamma$ interface. Because of our central *anatz* that the carbon is *locally in equilibrium* with both the α and γ phases at the interface, then we insist that the concentration makes a jump between $c^{\alpha\gamma}$ and $c^{\gamma\alpha}$ as indicated in figure 2. Way to the right in the austenite the carbon concentration is of course the nominal \bar{c} . We don't know the shape or the extent of the profile to the right of the interface so we take the simplest approach that the concentration decreases linearly away and after a distance Δz has reached the bulk concentration. To the left of the interface we know that the concentration in the growing ferrite is that given by the tie line in figure 1 which as indicated in figure 2 is $c^{\alpha\gamma}$.

We are trying to find the speed of the interface which will tell us the rate of growth of the ferrite at the expense of the vanishing austenite. This means we are seeking a formula for the quantity

$$v = \frac{\partial z^*}{\partial t}$$

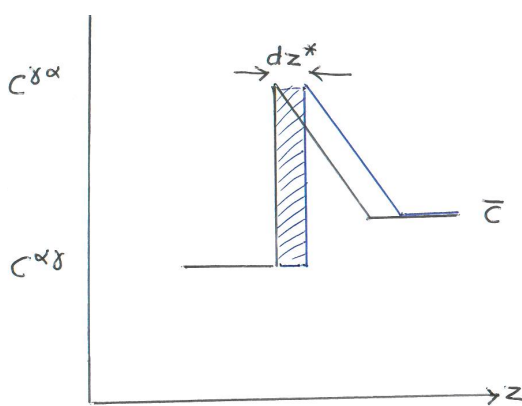


Figure 3

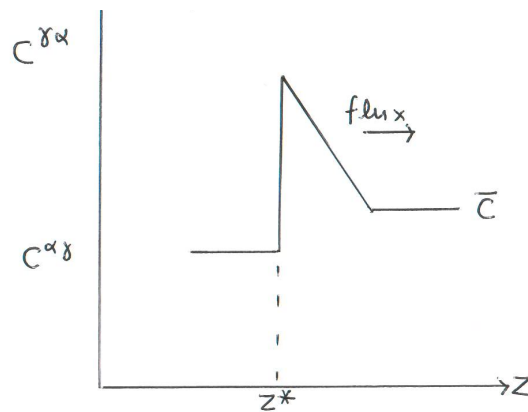


Figure 4

Consider figure 3: as the interface moves by an infinitesimal amount dz^* , an amount of carbon as indicated as the shaded rectangle must be moved to the front of the interface in order that the new ferrite created has a concentration $c^{\alpha\gamma}$. So if the interface is to move forward an amount dz^* in a time dt then the rate at which carbon is rejected into the austenite must be

$$\text{Rate of solute partitioning} = (c^{\gamma\alpha} - c^{\alpha\gamma}) \frac{\partial z^*}{\partial t} \tag{1.1}$$

The removal of carbon must happen by solid state diffusion in the austenite and Fick's first law tell us that the diffusive flux away from the interface is

$$\text{Diffusive flux away from interface} = -D \frac{\partial c}{\partial z} \tag{1.2}$$

When we equate (1.1) and (1.2), we get

$$(c^{\gamma\alpha} - c^{\alpha\gamma}) \frac{\partial z^*}{\partial t} = -D \frac{\partial c}{\partial z} \quad (1.3a)$$

$$\approx -D \frac{\bar{c} - c^{\gamma\alpha}}{\Delta z} \quad (1.3b)$$

where we have made the approximation of a linear profile as in figure 2. This is our equation for v , except that we don't know what to use for Δz . For the next step we invoke conservation of mass, as illustrated in figure 5. The areas of the triangle and the rectangle must be equal at all times: all of the carbon that existed in the austenite between $z = 0$ and $z = z^*$ having a concentration \bar{c} must have been pushed in front of the interface into the carbon enriched volume which extends in our model from $z = z^*$ to $z = z^* + \Delta z$, so that the ferrite will have its equilibrium concentration, $c^{\alpha\gamma}$. Note that as growth proceeds the volume of enriched carbon in the receding austenite gets larger, and since the height of the triangle remains constant at $c^{\gamma\alpha}$ it follows that the slope must be getting less because Δz is increasing with time. This means that the rate of growth must be slowing since the diffusive flux depends on the slope as in figure 4.

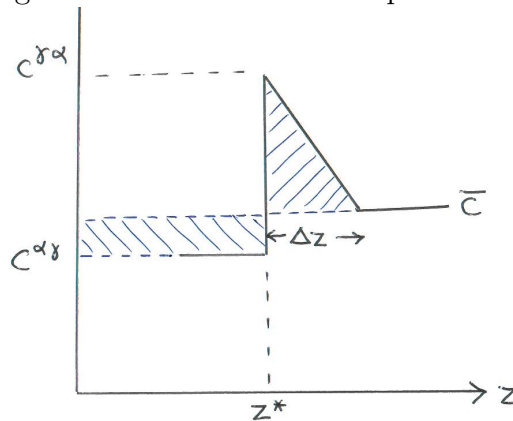


Figure 5: mass balance

Equating the two areas in figure 5 we see that mass balance requires

$$(\bar{c} - c^{\alpha\gamma}) z^* = \frac{1}{2} (c^{\gamma\alpha} - \bar{c}) \Delta z \quad (1.4)$$

Combining equations (1.3b) and (1.4) leads to

$$\frac{\partial z^*}{\partial t} = \frac{D (c^{\gamma\alpha} - \bar{c})^2}{2z^* (c^{\gamma\alpha} - c^{\alpha\gamma}) (\bar{c} - c^{\alpha\gamma})} \quad (1.5)$$

that is

$$z^* \propto \sqrt{Dt} \quad (1.6)$$

You see that the position of the interface goes like the square root of the time, so the rate of growth of the ferrite into the austenite slows down over time as we anticipated in the previous paragraph—as more and more of the carbon rejected from the growing ferrite piles up behind the α - γ interface, so the slope of the carbon concentration becomes less

and so the flux of carbon into the receding austenite is slowed, in accord with Fick's law.

2. Ternary Fe–Mn–C alloy

We now turn to a more interesting and challenging case: a ternary Fe–X–C alloy, where typically X could be Mn, Mo, Si, Co, Cu, Al, Cr, Ni and so on. We will take X to be Mn in what follows, just to fix our ideas.

In the single component case, by equating the rate of solute partitioning with the diffusive flux away from the α – γ interface we obtained for the speed, v , of the interface

$$(c^{\gamma\alpha} - c^{\alpha\gamma}) \frac{\partial z^*}{\partial t} = (c^{\gamma\alpha} - c^{\alpha\gamma}) v = -D \frac{\partial c}{\partial z}$$

You will agree that in the case of two components, say C and Mn, we will have

$$(c_C^{\gamma\alpha} - c_C^{\alpha\gamma}) v = -D_C^\gamma \frac{\partial c_C}{\partial z} \quad (2.1a)$$

$$(c_{Mn}^{\gamma\alpha} - c_{Mn}^{\alpha\gamma}) v = -D_{Mn}^\gamma \frac{\partial c_{Mn}}{\partial z} \quad (2.1b)$$

and we'll be asked to find solutions to these simultaneous equations that give up a single value of the speed, v . However the diffusivities of C and Mn in austenite differ by many orders of magnitude as you saw in **units 2A 2B, slides 22–24**.

$$D_C^\gamma \gg D_{Mn}^\gamma$$

while the other quantities in (2.1) are not likely to differ by more than a factor of ten. This would appear to present an insurmountable difficulty. But we are rescued by the extra degree of freedom in the phase diagram. The point is that in figure 1 we had no choice in placing the tie line in the binary phase diagram.

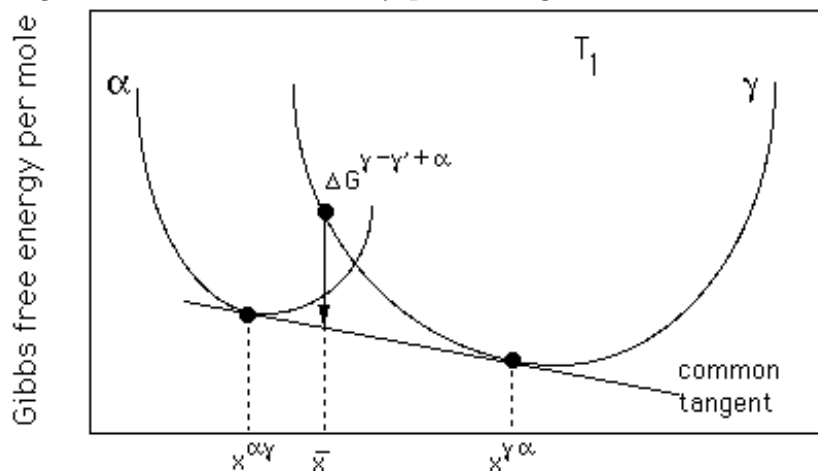


Figure 6

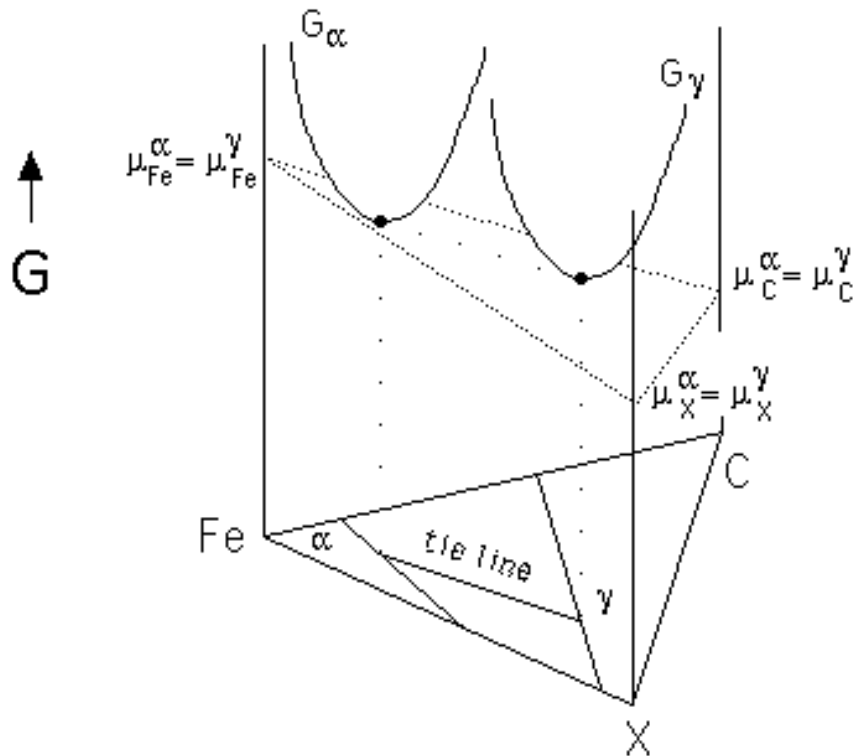


Figure 7

But compare figures 6 and 7. In the binary case, figure 6, there is only one common tangent to the two Gibbs free energy curves. In the ternary instance however, rather than being asked to find a *straight line* that makes contact with two two-dimensional *curves*, we need to find a *flat plane* that makes contact with two three-dimensional *surfaces*—like two upturned pudding bowls. Think a bit and you'll realise there's an infinity of ways to do this: you can place the plane (shown as a dotted triangle in figure 7) so that it touches both upturned Gibbs free energy surfaces and then roll and tilt it while it remains in contact with both. Of course in doing so we find an infinity of equilibrium situations, each having different values of the chemical potentials of the three components, although in every case the chemical potentials of each component are equal in the two phases.

As we rock the surface we produce an infinite number of tie lines in the two phase $\alpha + \gamma$ field that you see projected onto the base of the ternary phase diagram in figure 7. Some of these are indicated in figure 8.

We can now play games with equations (2.1). Since $D_C^\gamma \gg D_{Mn}^\gamma$ and the left hand sides are roughly the same order of magnitude, to make the right hand sides also the same order of magnitude we must *either* find a way to make the gradient of the Mn concentration, $\partial c_{Mn}/\partial z$ very, very large; *or* make the gradient of the carbon concentration $\partial c_C/\partial z$ very, very small. We do this by a judicious choice of tie line. We'll take the second choice first.

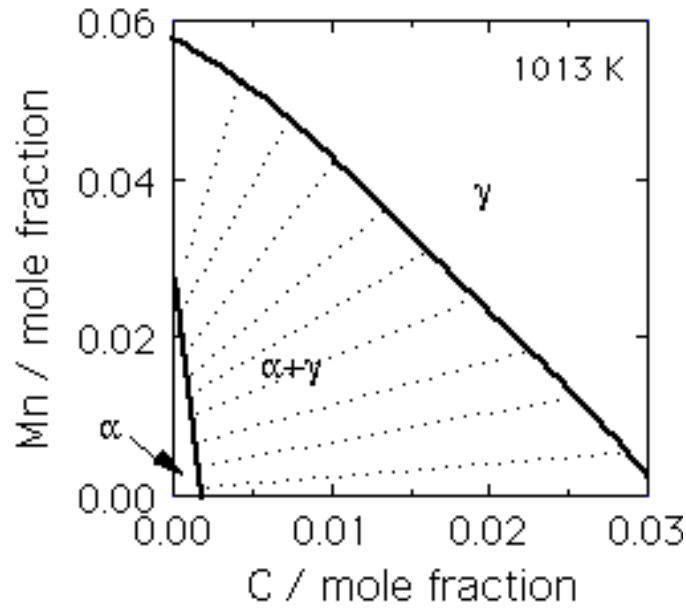


Figure 8

Look at figure 9. For this instance we choose an alloy composition and temperature that is close to the γ -field—that is, low undercooling. We choose the tie line like this: drop a perpendicular at the alloy composition indicated by the red dot and where it intersects the $\alpha + \gamma / \gamma$ phase boundary select the tie line that connects that same point to the α phase field. This is the lower of the two red lines. Now you see that the carbon concentration in equilibrium with γ , $c^{\gamma\alpha}$, is equal to the nominal composition, \bar{c} , and so the gradient of carbon concentration in the austenite is indeed small, even zero. The gradient of Mn concentration is now fixed by the difference in Mn concentrations at either end of the tie line. Equations (2.1) now have similar magnitude right hand sides and a unique value of the speed, v , may be deduced.

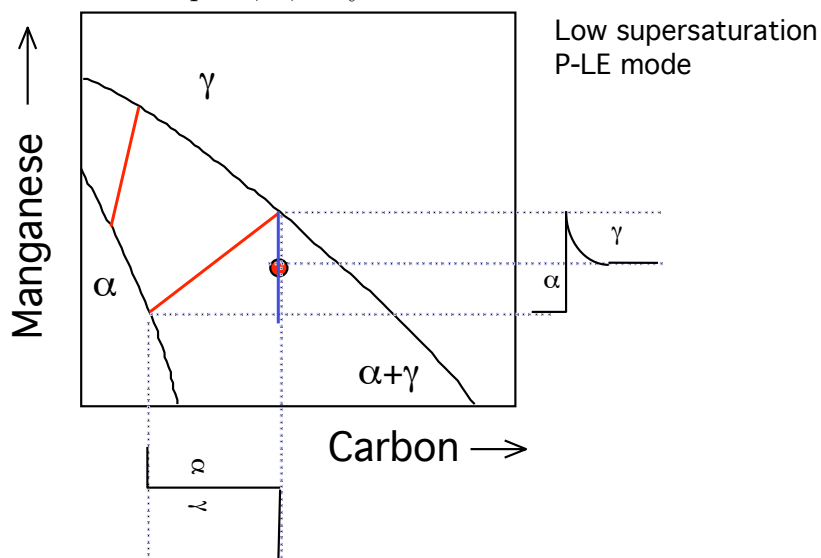


Figure 9

The alternative strategy is illustrated in figure 10. This is a case of rather larger undercooling for which we adopt the opposite approach: we try and make the gradient of Mn

concentration $\partial c_{\text{Mn}}/\partial z$ very large. To do this we now construct a horizontal line (the broken blue line) and where it intersects the $\alpha / \alpha + \gamma$ phase boundary, that's the tie line we choose. Now the Mn concentration is *roughly the same in both phases*; however while the concentration in the austenite is same as in the ferrite, by the assumption of local equilibrium it has to have the value at the interface as dictated by the intersection of the tie line with the $\alpha + \gamma / \gamma$ boundary. The result is a huge spike in Mn and consequently a large gradient as indicated at the right of the figure. The carbon has to follow the values of $c^{\alpha\gamma}$ and $c^{\gamma\alpha}$ using the chosen tie line and there now results a significant gradient as indicated at the bottom of figure 10.

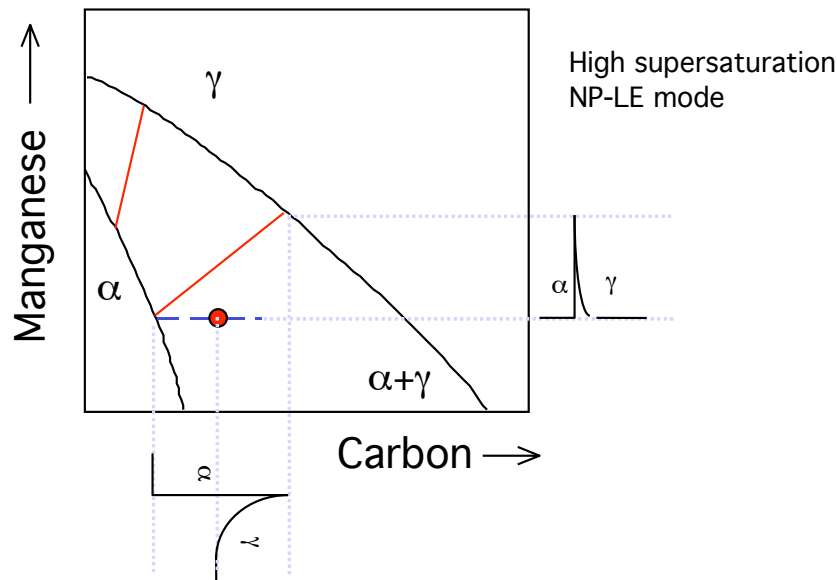


Figure 10

You might ask, how do I know to make a vertical or horizontal construction? Well, examine figure 9: if I made a horizontal line through the red dot and so selected a tie line similar to the one illustrated to the left, then see what happens. The carbon concentration at both ends is *less than* the bulk composition. So this doesn't satisfy mass conservation: the carbon concentration can't be less than \bar{c} in both phases. Similarly if I made a vertical construction in figure 10 then the tie line I would get would require there to be *more* Mn in both ferrite and austenite that was originally in the alloy. Again, impossible. The alloy really only has one choice at an isothermal transformation, depending on temperature and composition. This is illustrated in **slides 17 and 18**. This choice gives rise to two possible growth modes, "partitioning local equilibrium" (P-LE) and "negligible partitioning local equilibrium" (NP-LE). Only one tie line can achieve the correct gradients of Mn and C to permit a single v to a solution of equations (2.1). The alloy does not choose exactly a vertical or horizontal line, but chooses the tie line that results in a growth mode that honours the local equilibrium condition. To be more precise we should accept that the flux is proportional not to *concentration* but to *activity* gradients and this is illustrated in figures 11 and 12.

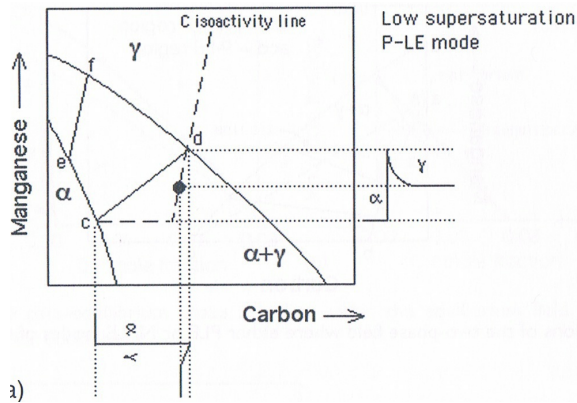


Figure 11

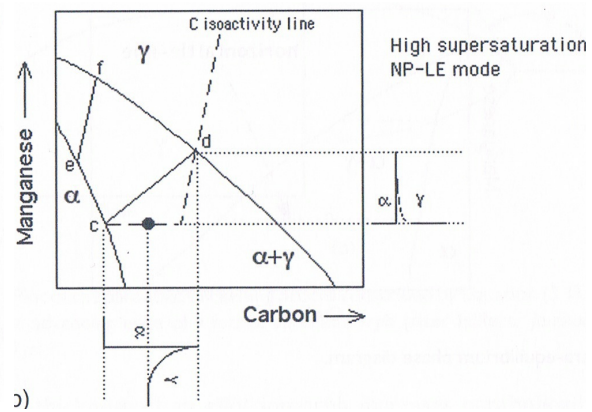


Figure 12

So, P-LE is characterised by a low undercooling; the carbon diffuses slowly because the carbon gradient is vanishingly small and the growth speed is dominated by Mn diffusion which is necessarily slow. Integration of (1.5) shows that

$$v \propto \sqrt{\frac{D}{t}} \quad (2.2)$$

and here the relevant diffusivity is that of the *substitutional* element. NP-LE is a faster growth mode because although Mn has to diffuse short distances to maintain the spike in concentration at the interface, the Mn concentration in the ferrite and austenite is the same, namely the bulk concentration—so there is no long ranged diffusion of Mn and the growth mode is fast, being controlled by the carbon diffusivity: in this case in (2.2) we would use the carbon diffusivity. This orders-of-magnitude higher speed is consistent with the larger undercooling. The spike in concentration is actually observed in some instances. On the other hand the alloy may choose to abandon the local equilibrium and simply maintain the Mn concentration at a uniform level everywhere. If the carbon continues to respect local equilibrium and the carbon partitions into equilibrium concentrations in both ferrite and austenite then this mode of growth is called *paraequilibrium*.[†] In paraequilibrium only the carbon is in equilibrium and the Mn (and other substitutional elements) is out of equilibrium. This is a faster growth mode than P-LE and NP-LE since the rate is determined only by carbon diffusivity; the alloy has to pay the price of a higher Gibbs free energy for the non equilibrium state.

Figure 13 shows schematic concentration profiles of carbon and substitutional elements in a hierarchy of growth modes in steel. The first two show carbon and substitutional element profiles in the P-LE and NP-LE modes described above. The lower three do not respect local equilibrium at the interface: in paraequilibrium only the carbon is in local equilibrium; in the lowest two, the concentrations of no element are in equilibrium. A martensitic transformation is defined as one for which there is no change of composition between parent and product phase and hence no accompanying diffusion, see **units 2A 2B, slide 26**.

[†] Local equilibrium is sometimes called *ortho-equilibrium* but this usage is now outdated.

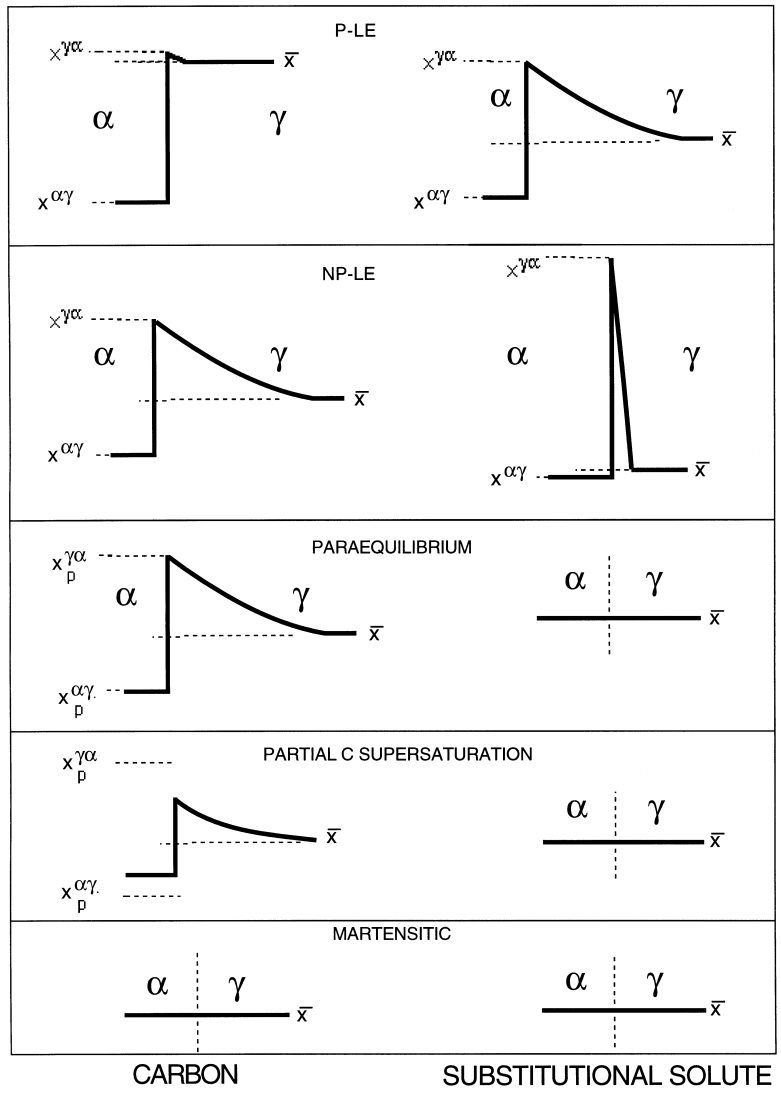


Figure 13

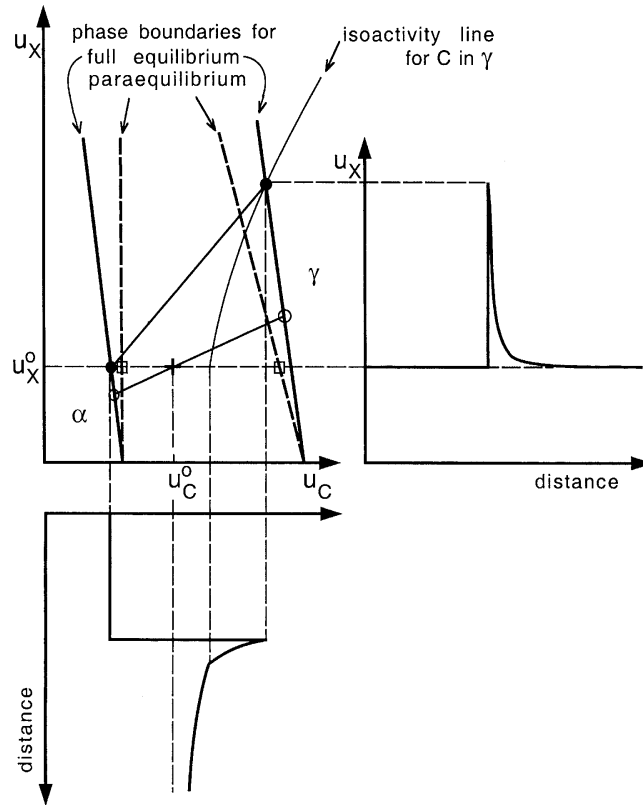


Figure 14: from M. Hillert and J. Ågren, *Scripta Mat.*, **50**, 697 (2004)

Figure 14 illustrates the contrast between NP-LE and paraequilibrium. The tie lines in paraequilibrium are horizontal and the paraequilibrium phase boundaries lie entirely within the equilibrium phase boundaries as shown in figure 15. The reason for this is that at zero Mn concentration (along the abscissa) the $\alpha / \alpha + \gamma$ and $\alpha + \gamma / \gamma$ phase boundaries are those from the binary Fe–C phase diagram and whether equilibrium or paraequilibrium pertains is irrelevant in the binary case; at zero carbon concentration, in paraequilibrium, the concentration of Mn is the same in both ferrite and austenite and hence the phase boundaries coincide as shown in figure 15.

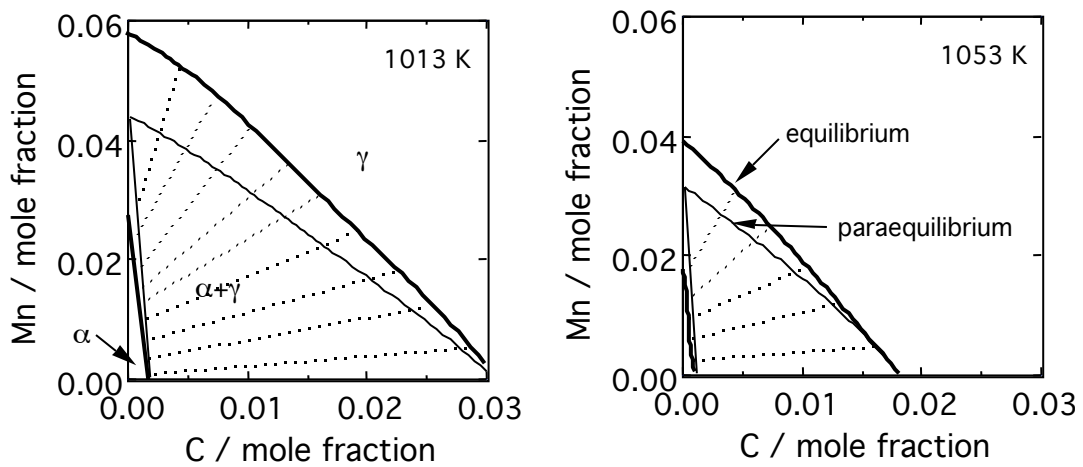


Figure 15

I am very grateful to Professor Sir Harry Bhadeshia for giving me access to his lecture notes.

Further reading

<https://www.youtube.com/watch?v=CUvWB402fL8>

<https://www.youtube.com/watch?v=XruMVfICSV4>

H. K. D. H. Bhadeshia and R. W. K. Honeycombe, "Steels: Microstructure and Properties," Elsevier, 3rd Edition, 2006

H. K. D. H. Bhadeshia, "Bainite in Steels", Maney Publishing; 3rd Edition edition (2015); 2nd edition is available free at <http://www.msm.cam.ac.uk/phase-trans/newbainite.html>

Problems

- 1 Consider the growth of ferrite from austenite in the binary iron–carbon system. Use a tie line in a sketch showing the extrapolated phase boundaries in the Fe–C phase diagram to define the quantities $c^{\alpha\gamma}$ and $c^{\gamma\alpha}$ which are respectively the interface concentrations of carbon in the ferrite in equilibrium with austenite, and in austenite in equilibrium with ferrite. Then draw a concentration profile of carbon at the moving α – γ interface assuming a linear decrease over a distance Δz ; indicate on your plot the quantities $c^{\alpha\gamma}$ and $c^{\gamma\alpha}$, and the nominal carbon concentration in the steel, \bar{c} . Mark the position of the interface as z^* . Write down formulas for the rate of solute partitioning and the diffusive flux away from the interface and by equating these, after taking into account the conservation of mass, show that

$$v = \frac{\partial z^*}{\partial t} = \frac{D (c^{\gamma\alpha} - \bar{c})^2}{2z^* (c^{\gamma\alpha} - c^{\alpha\gamma}) (\bar{c} - c^{\alpha\gamma})}$$

where D is the diffusivity of carbon in austenite, and v is the speed of the moving interface.

Now go forward and consider the ternary Fe–C–Mn system. The previous analysis will result in two coupled equations each containing the common interface speed, v , namely

$$\begin{aligned} (c_C^{\gamma\alpha} - c_C^{\alpha\gamma}) v &= -D_C^\gamma \frac{\partial c_C}{\partial z} \\ (c_{Mn}^{\gamma\alpha} - c_{Mn}^{\alpha\gamma}) v &= -D_{Mn}^\gamma \frac{\partial c_{Mn}}{\partial z} \end{aligned}$$

Explain why it is not in general easy to find a solution for v . Indicate how solutions can be found by exploiting the extra degree of freedom offered by the ternary phase diagram which allows you a choice of tie line compared to the first figure that you drew. Make **two** projections of the phase diagram having carbon and manganese concentrations along the abscissa and ordinate, and use these to illustrate the two possible modes of local equilibrium growth: *partitioning local equilibrium* (P-LE) at low supersaturation (little undercooling) and *negligible partitioning local equilibrium* (NP-LE) at high supersaturation (large undercooling). Using a third diagram, explain why it is not possible for P-LE to occur at large undercooling; and using a fourth diagram explain why it is not possible for NP-LE to occur at small undercooling.

In view of the above, explain the affect that Mn can have on the position of the “nose” of the TTT diagram when comparing the Fe–C and Fe–C–Mn alloy systems.

What is meant by *paraequilibrium*? Draw a projection in sketch of the Fe–C–Mn phase diagram to indicate the phase boundaries and a few representative tie lines in equilibrium and in paraequilibrium.

Lecture 5

5–2 Bainite

To continue the theme of the decomposition of austenite we turn now from reconstructive to displacive transformation. Look again at **slide 12** in **lecture 2**. Christian does not actually classify in terms of reconstructive and displacive, probably because these terms are not clearly defined. Let us agree that in a *displacive* transformation in steel, at least the iron atoms move over distances no greater than on the order of the lattice constant. This then in steel covers martensite in which no atoms diffuse, and bainite in which the carbon probably diffuses if not during transformation to ferrite but certainly within times of order one second afterwards. It is nowadays thought by most people that bainite forms very much like martensite by a military transformation characterised by a habit plane and orientation relation (see **lecture 7**) but that it is nevertheless diffusion controlled and not athermal[‡] since the rate of transformation is governed by the diffusion of carbon and is thereby thermally activated. We will discuss martensite in detail in **lecture 7**, so jumping ahead for the moment, let us assert that the transformation to bainite resembles that of martensite in its crystallography. However the transformation is accompanied by significant carbon diffusion so that after transformation, in contrast to martensite, the resulting phase has a different composition (at least in regard to carbon) compared to the parent austenite. The question that is still hotly debated is whether the carbon diffusion occurs simultaneously with the γ to α transition or whether it occurs afterwards, albeit within a very short amount of time. I will encourage you to adhere to the latter view (associated with the names of Bhadeshia, Edmonds, Christian and others) rather than the former (associated with the names of Hillert and Aaronson). At all events everyone agrees that there are two principal forms of bainite. At higher growth temperatures the diffusion length is sufficient that carbon is rejected completely from the growing ferrite and appears as cementite precipitated in between the bainite laths or plates, possibly within any retained austenite. This is called upper bainite. At lower temperatures the carbon precipitates as cementite within the bainitic ferrite forming a typical habit at 60° to the longitudinal axis of the lath or plate. This is called lower bainite.

If we take it that, at least in the first instance, the α and γ have the same composition then we see from **slide 4** that this involves a vertical shift in the free energy–composition diagram. If, conversely, the transformation were reconstructive then the resulting phases would have compositions at either ends of the tie line. This means that unlike in the case of reconstructive growth of ferrite as discussed in **lecture 4** the free energy must decrease in changing from γ to α and this is only possible if the nominal composition \bar{x} is to the left of the intersection of the α and γ free energy curves (**slide 5**). This particular value of carbon concentration depends on temperature since the free energy

[‡] Athermal means the amount transformed depends on *temperature* but not on *time*. This is the converse of a thermally activated process whose signature is that at a given temperature the amount transformed depends on the elapsed time, dictated by the kinetics of the reaction.

curves are temperature dependent. The value of this critical carbon concentration when plotted against temperature in the Fe–C phase diagram is called the “ T_0 line” and it falls in between the extrapolated “no-name” and Ae_3 lines as indicated in **slide 5**.

To return to the controversy surrounding what controls the growth of bainite, let me quote Christian. “Micrographs of upper bainite are all consistent with partitioning of the carbon to the austenite prior to carbide precipitation . . . What is not clear is whether segregation accompanies growth, and indeed controls the growth rate, or whether it follows the rapid diffusionless growth of individual sub-units of the ferrite structure.” One way to test the two hypotheses is to isothermally transform at a given temperature and measure the carbon concentration in the retained austenite. Christian continues, “There are then two possibilities, either two-phase (metastable) equilibrium has been attained between the ferrite and the austenite or the carbon concentration has risen to a level at which diffusionless growth of ferrite is no longer possible. In the first case, the mean carbon concentration of the austenite after growth has ceased would be expected to correspond approximately to the Ae'_3 or Ae''_3 curve whereas in the second case, this content should be close to the T_0 or T'_0 curve.”[†] What this means is that bainitic ferrite will continue to grow and reject carbon into the surrounding austenite which becomes increasingly enriched in carbon until it can no longer transform. If the transformation were by equilibrium partitioning then growth would cease when the carbon concentration in the austenite (take this to be \bar{x} in **slide 4**) reaches a value near $x^{\gamma\alpha}$, that is, near the Ae_3 extrapolated phase boundary. On the other hand if the transformation is diffusionless then it would cease much earlier, namely when the composition of carbon in the remaining austenite reaches the T_0 or T'_0 line since beyond that composition the γ has a lower free energy than the α so has no motivation to transform at the same composition. **Slide 5** borrowed from Bhadeshia shows this in a cartoon: at any temperature little green bainitic ferrite laths or plates grow, rejecting carbon (black arrows) into the surrounding austenite which increases accordingly in carbon concentration *until* this reaches the T'_0 line at *that temperature*. Measurements of the carbon concentration in retained austenite support this hypothesis. Carbon concentrations greater than that at T'_0 are *not* observed in bainite, but they *are* observed in Widmanstätten ferrite (**slide 8**).

Slides 9–14 are taken from a paper by Babu and Bhadeshia concerning acicular ferrite. This is a microstructure, often associated with weldments, designed particularly to impart toughness. In contrast to earlier thinking, it is now recognised that acicular ferrite is nothing other than bainite that has nucleated in the grain interiors rather than at grain boundaries.

[†] Ae'_3 means the paraequilibrium Ae_3 , and Ae''_3 means the paraequilibrium Ae_3 accounting for strain. T'_0 means T_0 after accounting for strain.

5-3 Alloy steels

We now start our discussion of alloy steels. Alloying elements are classed broadly into austenite and ferrite stabilisers. **Slide 17** shows the principal elements in steel separated in this way. Actually rather than two, there are four classes of element depending on the topology of their equilibrium diagram with iron. The four types are illustrated in **slide 18**. Here are the characteristics of the four and some of the elements that are responsible.

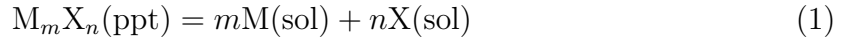
1. **Open γ -field** (Type A-1). Ni, Mn; also Co, Ru, Rh, Pd, Os, Ir, Pt. Enables metastable austenite. No Fe-rich compounds
2. **Expanded γ -field** (Type A-II). Most important: C, N. Range limited by Fe-rich compound formation. Also Cu, Zn, Au.
3. **Closed γ -field** (Type B-1). α -stabilisers contract the γ -field into a “ γ -loop”. α and δ fields become continuous. Alloys beyond the loop are *not heat treatable*. Si, Al (also inhibit cementite formation). Be, P, Sn, Sb, As and carbide forming elements Ti, V, Mo, Cr, W.
4. **Contracted γ -field** (Type B-II). The loop is interrupted with two-phase fields of Fe-rich compounds. Boron most significant. Also S, Ce and carbide forming elements Ta, Nb, Zr.

Characteristic of alloy steels is the occurrence of second phase transition metal carbides, nitrides or carbonitrides in the microstructure. They play two principal roles. (*i*) those that are not very soluble in austenite (roughly speaking those with a more negative enthalpy of formation) will persist at annealing temperatures and act as austenite grain refiners. (*ii*) Those that are more soluble will dissolve fully in austenite and the elements in solid solution will be available to produce fine precipitates as particle hardeners in the heat treated microstructure (see **lecture 1**). **Slide 19** ranks some common transition metal carbides and nitrides according to their enthalpy of formation. **Slide 20** shows some effects of microalloying on recrystallisation behaviour and **slide 21** the efficacy of three carbides with differing solubilities as austenite grain refiners. **Slide 22** is to remind you that grain refinement is a consequence of grain boundary pinning by the so called Zener effect.

Solubility product. We need to quantify the solubility of different transition metal carbides and nitrides, particularly in austenite at high temperature. This is because transition metal carbides play two crucial roles in microalloy and low alloy steels. (*i*) The more *insoluble* precipitates, for example TiC, NbN, exist at high temperature and act as austenite grain refiners, say, during hot rolling. (*ii*) The more *soluble* compounds, for example V_4C_3 or VC, Mo_2C and chromium carbides, will enter solution in the austenite during annealing and can be precipitated as nano-precipitates to improve strength during cooling and transformation to ferrite, say, by interphase precipitation, or during tempering after a quench to strengthen martensite. Iron carbide is the most soluble of all. Actually the more soluble compounds are those having the smaller enthalpies of

formation (see **slide 19**). The alloy designer needs mathematical models and data that can be used to predict the distribution of carbon, nitrogen and transition metal alloying elements as functions of temperature—how much is in solution and how much exists as precipitates? We'd also like to know the size, shape, habit and orientation relation, but that's another matter.

Consider a chemical reaction



which describes the dissolution of a carbide or nitride $M_m X_n$ precipitate (ppt), for example NbN or V_4C_3 into solution (sol) in austenite at some temperature T . In equilibrium the chemical potentials of M and X are the same in the precipitate and in the solution, so we have

$$\mu_{M,\text{ppte}} = \mu_{M,\text{sol}} \quad \text{and} \quad \mu_{X,\text{ppte}} = \mu_{X,\text{sol}} \quad (2)$$

Expressing the chemical potentials in the usual way in terms of standard chemical potential and activity, this becomes

$$\begin{aligned} \mu_{M,\text{ppte}}^\circ + RT \ln a_{M,\text{ppte}} &= \mu_{M,\text{sol}}^\circ + RT \ln a_{M,\text{sol}} \\ \mu_{X,\text{ppte}}^\circ + RT \ln a_{X,\text{ppte}} &= \mu_{X,\text{sol}}^\circ + RT \ln a_{X,\text{sol}} \end{aligned}$$

Now, the chemical potential of the precipitate is, in view of (1) and (2)

$$\begin{aligned} \mu_{\text{ppte}} &= m\mu_{M,\text{ppte}} + n\mu_{X,\text{ppte}} \\ &= m\mu_{M,\text{sol}} + n\mu_{X,\text{sol}} \end{aligned}$$

and therefore, again in terms of activity and standard state,

$$\mu_{\text{ppte}}^\circ + RT \ln a_{\text{ppte}} = m\mu_{M,\text{sol}}^\circ + mRT \ln a_{M,\text{sol}} + n\mu_{X,\text{sol}}^\circ + nRT \ln a_{X,\text{sol}}$$

and rearranging this last equation, I get,

$$RT (m \ln a_{M,\text{sol}} + n \ln a_{X,\text{sol}} - \ln a_{\text{ppte}}) = \mu_{\text{ppte}}^\circ - m\mu_{M,\text{sol}}^\circ - n\mu_{X,\text{sol}}^\circ$$

which is

$$\begin{aligned} RT \ln \frac{a_{M,\text{sol}}^m a_{X,\text{sol}}^n}{a_{\text{ppte}}} &= -\Delta G_{\text{sol}}^\circ \\ &= RT \ln K \end{aligned}$$

having defined

$$\Delta G_{\text{sol}}^\circ = m\mu_{M,\text{sol}}^\circ + n\mu_{X,\text{sol}}^\circ - \mu_{\text{ppte}}^\circ$$

as the standard free energy of solution of the precipitate. This equation also serves to define the *equilibrium constant* K for the chemical reaction. I now have

$$a_{M,\text{sol}}^m a_{X,\text{sol}}^n = a_{\text{ppte}} \exp(-\Delta G_{\text{sol}}^\circ/RT)$$

The activity of a pure defect-free solid phase is constant (usually taken to be one) and for a dilute solution Henry's law tells us the the activity of a solute is proportional to

the concentration x expressed as an atomic fraction. The proportionality constants, γ , are called *activity coefficients* and are constant, independent of temperature and composition. So if x_M and x_X are the concentrations of M and X in the solid solution and γ_M and γ_X are activity coefficients, we now have

$$(\gamma_M x_M)^m (\gamma_X x_X)^n = a_{\text{ppte}} \exp(-\Delta G_{\text{sol}}^\circ/RT)$$

I can gather the three constants into a single constant, say, $C = a_{\text{ppte}}/\gamma_M^m \gamma_X^n$, and write

$$x_M^m x_X^n = C \exp(-\Delta G_{\text{sol}}^\circ/RT)$$

The *weight percentages* of M and X, which we conventionally write as [M] and [X] are proportional to the concentrations so the previous equation is equivalent to

$$[M]^m [X]^n = D \exp(-\Delta G_{\text{sol}}^\circ/RT)$$

in which D is another constant involving the atomic weights of the components and factors of a hundred to convert to percent. I find

$$D = C \times 100^2 \frac{(m+n)^2}{m^2 A_M/A_X + 2mn + n^2 A_X/A_M}$$

where A_M and A_X are the relative atomic masses (or atomic weights) of the elements M and X. All this *defines* the *solubility product*, k_s ,

$$\begin{aligned} k_s &= [\text{wt}\%M]^m [\text{wt}\%X]^n \\ &= [M]^m [X]^n \\ &= D \exp(-\Delta G_{\text{sol}}^\circ/RT) \end{aligned} \quad (3)$$

Now I take logarithms to the base ten on both sides and I get

$$\log k_s = A - B/T \quad (4)$$

where the constants are

$$A = \log D \quad \text{and} \quad B = \Delta G_{\text{sol}}^\circ/2.303R$$

Then all the constants including changes from natural to base 10 logs, standard states and conversions to weight percent are accounted for by fitting experimental data to equation (4). You will always find solubility product data in the metals handbooks and literature given by quoting the constants A and B for a particular carbide or nitride in austenite or ferrite. Of course the whole thing can be extended to multicomponent precipitates, for example (V,Mo)(C,N) a carbonitride of vanadium and molybdenum (see **lecture 6, slides 17 and 18**) but it's a mess to write down and problems such as on the next page require a computer to solve.

Because of equation (4) if we plot $\ln k_s$ (or $2.303 \log k_s$) against $1/T$ we get a straight line with a negative slope of magnitude $\Delta G_{\text{sol}}^\circ/R$. This is called an *Arrhenius plot*; an example is in **slide 25**.

On the other hand, because of equation (3) it is clear that plotting $[\text{wt}\%M]^m$ against $[\text{wt}\%X]^n$ at any given temperature will result in a curve resembling a hyperbola as shown, for example, in the schematic in **slide 26**. The way to interpret this graph is as follows. At the required temperature, say T_2 , and given concentrations of M and X (these could be, say, vanadium and nitrogen) we wish to know how much of the vanadium and nitrogen are in solution and how much are tied up in vanadium nitride precipitates. If we place a point on the graph corresponding to the known nominal compositions then *in equilibrium* if that point falls to the left and below the curve the microstructure will be a single phase austenite with V and N in solution. If the point falls above and to the right of the hyperbola then the microstructure will be a two phase mixture of VN and austenite solid solution. The curve is therefore a graph of the *solubility limit* at that temperature—if the concentrations of V and N lie on a point to the right and above the solubility limit the that limit is exceeded and some of these elements must come out of solution and form precipitates.

Of course the next question is, *how much precipitate do I expect?* The valuable predictive power of the solubility product is outlined in **slides 27–29**. It's actually quite simple. Take the example of vanadium nitride. We first define these quantities.

V_T : wt% V in alloy

N_T : wt% N in alloy

$[V]$: wt% V dissolved in austenite

$[N]$: wt% N dissolved in austenite

V_{VN} : wt% V present as VN

N_{VN} : wt% N present as VN

A_V : relative atomic mass of V

A_N : relative atomic mass of N

Then it's easy to see by the mass balance that the total weight percentages of vanadium and nitrogen are the sum of the amounts in solution plus that tied up up in the precipitates, leading to

$$V_T = [V] + V_{VN} \quad (5)$$

$$N_T = [N] + N_{VN} \quad (6)$$

The *atomic* percentages of V and N tied up in VN are equal because of stoichiometry. So the *weight* percentages are in the ratio of the atomic weights, leading to

$$N_{VN} = V_{VN} \frac{A_N}{A_V} \quad (7)$$

And, by definition of the solubility product we have

$$k_s = [V][N] \quad (8)$$

The rest is algebra. First we expand out equation (8) using (5) and (6) and then substituting (7),

$$\begin{aligned}
 k_s &= [V][N] \\
 &= (V_T - V_{VN})(N_T - N_{VN}) \\
 &= (V_T - V_{VN}) \left(N_T - V_{VN} \frac{A_N}{A_V} \right) \tag{9}
 \end{aligned}$$

The quantity we are looking for is V_{VN} , the weight percentage of vanadium tied up as precipitate. From that we can then work out how much vanadium and how much nitrogen remain in solution by the mass balance equations (5) and (6). So, first expand out equation (9) and see that it amounts to a quadratic equation in V_{VN} for which apply the standard formula.

$$\begin{aligned}
 V_{VN} = \frac{1}{2} \frac{A_V}{A_N} & \left[\left(N_T + V_T \frac{A_N}{A_V} \right) \right. \\
 & \left. - \sqrt{\left(N_T + V_T \frac{A_N}{A_V} \right)^2 - 4 \frac{A_N}{A_V} (V_T N_T - k_s)} \right]
 \end{aligned}$$

This achieves our goal. We have V_{VN} as a function of the nominal compositions of V and N and their atomic weights; and the solubility product which is a measurable function of the temperature. If we had more than one possible compound, or if we are interested in carbonitrides then the thermodynamic principles remain the same. The algebra becomes a lot more complicated and requires the solution of a number of simultaneous equations. The alloy designer uses commercial computer packages.

Now examine **slide 30**. This illustrates in part the perennial problem arising from the unfortunate fact that metallurgists always work in weight percent, whereas the physics and chemistry of course refers to atom percent—because atoms combine one to one in chemical reactions and so on. If the stoichiometry were one to one (which we assume in all the examples here) and if we were plotting *atomic percent* not *weight percent* then all points lying on a 45° diagonal would represent stoichiometric compositions. Because we actually plot weight percent then the stoichiometric line has a slope given by the ratio of the atomic weights of the two components. Now suppose we are interested in austenite with nominal concentrations of vanadium and nitrogen indicated by the point P. We construct a line with the same slope as the stoichiometric line that passes through P and it does not intersect the origin because in general an alloy does not contain equal atomic percentages of V and N. Using this construction we take the intersection of the stoichiometric line passing through P with the solubility limit curve and at the intersection we read off the concentrations of V and N that remain in solution in the austenite.

Slides 31–37 are examples of solubility limit, or solubility product, curves for a number of microalloying elements in austenite. As I have mentioned, the importance of this cannot be overemphasised as it allows the materials engineer to design alloy compositions and heat treatment schedules to obtain a desired microstructure and hence desired

mechanical properties. In particular this gives control of austenite grain refiners and solution and reprecipitation to achieve particle hardening by interphase precipitation (**lecture 6**) or through tempering.

Slide 38 illustrates what you have learned up to now in this lecture. Suppose you are interested, for the sake of simplicity, in a steel with a single microalloying element, titanium, at 0.1 wt%. How can you optimise hardening precipitates that form after cooling from austenite by varying the carbon concentration? The upper diagram shows solubility limits (products) at three temperatures. Imagine that the steel requires an isothermal anneal at 1200° during which all the Ti and C are to be dissolved so that they can subsequently form, say, interphase precipitates as the austenite transforms to ferrite on cooling. You will need at least a stoichiometric amount of carbon or there won't be enough to tie up all the Ti as TiC and some Ti must inevitably remain in solution in the austenite and in the resulting ferrite—this may be fine if you are seeking some solution hardening (**lecture 1**). This is the situation if the carbon concentration falls in region A in the lower diagram. As the carbon increases from zero the amount of Ti and C that will be available to combine will increase until the stoichiometric line intersects the Ti concentration. Note that as we increase the carbon concentration the equivalent of our point P in **slide 30** is moving to the right along the horizontal broken line in the upper diagram. In region A there is more Ti than C atomic percent; beyond the stoichiometric point there is more C than Ti atomic percent. Therefore in region B, the amount of carbide that can form is fixed and at its maximum amount, given the 0.1 wt% of Ti; the remaining carbon will probably form iron or other carbides on cooling—no bad thing, perhaps. At the boundary of regions B and C the point P moves from the left and below the solubility limit to above and to its right so that at the soaking temperature of 1200° the equilibrium microstructure is austenite plus TiC. This means that not all the Ti and carbon become dissolved and that TiC that forms at the 1200° is likely to grow coarse and be useless at particle hardening. At the same time these coarse precipitates tie up some of the Ti and C that would otherwise be available to form fine interphase precipitates and in consequence the cooled alloy will have the TiC fraction “limited by solubility”. The conclusion is that in this case using any carbon concentration in the range of region B will give optimum fine carbide fraction, since if the carbon concentration is less the carbide fraction is limited by stoichiometry and if it's greater some Ti and C will be tied up as useless (possibly even deleterious) large second phase particles.

Slide 39 show how these ideas are exploited in the design of fine grain microalloyed niobium steels. Notice that there are two effects of increasing the annealing temperature before air cooling. (i) The yield stress increases overall. (ii) The Hall-Petch slope increases. This is because at the higher annealing temperatures, more NbC is dissolved and is therefore available for interphase precipitation in the ferrite in order to contribute to the particle hardening.

Further reading

<https://www.youtube.com/watch?v=nFLktGgjWhw>

<https://www.youtube.com/watch?v=kLPsk6Tpaig>

H. K. D. H. Bhadeshia and A. R. Waugh, *Acta Metall.*, **30**, 775 (1982)

S. S. Babu and H. K. D. H. Bhadeshia, *Materials Trans. JIM*, **32** 679 (1991) [uploaded to the Blackboard.]

My discussion of solubility product follows closely the treatment in T. Gladman, “The physical metallurgy of microalloyed steels,” Maney Publishing (Institute of Materials) 1997. Unfortunately this book is now out of print. But if you can get hold of a copy then do so.

R. W. K. Honeycombe, “Steels: Microstructure and Properties,” Edward Arnold, 1st Edition, 1981

K. G. Denbigh, “The principles of chemical equilibrium,” 4th edition, Cambridge University Press, 1981

D. R. Gaskell, “Introduction to metallurgical thermodynamics,” 2nd edition, McGraw-Hill, 1981

T. N. Baker, *Mat. Sci. Technol.*, **25**, 1083 (2009)

<https://www.youtube.com/watch?v=mKDveUFQcEU>

<https://www.youtube.com/watch?v=jnz3w81L13U>

H. K. D. H. Bhadeshia, “Bainite in Steels”, Maney Publishing; 3rd Edition edition (2015); 2nd edition is available free at <http://www.msm.cam.ac.uk/phase-trans/newbainite.html>

H. K. D. H. Bhadeshia and J. W. Christian, *Met. Trans.*, **21A**, 767 (1990)

Problems

- 5.1 Write notes to describe the principal similarities and differences when comparing *upper bainite*, *lower bainite* and *acicular ferrite*.
- 5.2 Provide evidence to show that the growth of bainite sheaves is not accompanied by any diffusion.
- 5.3 What is the meant by solubility product in the context of the physical metallurgy of steel?

- (i) Explain how the consideration of a dissolution reaction leads to a formula for an equilibrium constant in terms of chemical potentials and indicate the approximations that are made that lead to the metallurgical definition of solubility product, having the form

$$k_s = [\text{wt}\%M]^m [\text{wt}\%X]^n$$

- (ii) In view of your answer in (i) explain why the experimentally determined solubility product can be parameterised into the form

$$\log k_s = A - \frac{B}{T}$$

where T is absolute temperature and A and B are fitting parameters.

- (iii) The solubility product of vanadium nitride, VN, in austenite has been assessed and the constants found to be $A = 3.46$ and $B = 8330$. If austenite containing 0.1 wt% vanadium is to be annealed at 1000°C what is the maximum concentration of nitrogen that is permitted in order to avoid precipitation of VN during the anneal?
- (iv) If the nitrogen content of the austenite of (iii) is exceeded, explain how this can lead to grain refinement of the austenite during the 1000° C anneal. In your answer, explain how *Zener pinning* works.
- (v) Upon cooling following annealing of the steel in (iv) the austenite will transform to ferrite. Explain what is meant by *interphase precipitation* and describe what benefit the precipitation of VN would contribute to the mechanical properties of the steel. How could this property be modified by controlling the isothermal transformation temperature of the transformation from austenite to ferrite?

Lecture 6

The production of fine transition metal carbide precipitates is central to the particle strengthening of microalloy steel. This may occur after or, more commonly, during the isothermal or continuous cooling of austenite and its transformation to ferrite. We consider the precipitation of microalloy carbides under three headings.

1. **Precipitation in austenite.** Carbides are very reluctant to precipitate during soaking above A_3 even after days of holding at temperature. However if the steel is hot rolled in an austenite field of the phase diagram then carbides will precipitate because of the appearance of dislocations on which the precipitates can nucleate. **Slide 2** shows the typical C-curve kinetics of NbN precipitation after 50% reduction in thickness, and demonstrates the role of Mn in retarding the precipitation. It is said that this is due the effect of Mn in reducing the activity of the free nitrogen. The principal role of carbide, nitride and carbonitride precipitation in austenite is to refine the γ -grain size and hence set the scale for the final low temperature microstructure. **Slides 3 and 4** are taken from Peng *et al.* (2016) and show high resolution images of NbC precipitates resulting from thermomechanical heat treatment, schedule C.
2. **Precipitation during the $\alpha \rightarrow \gamma$ transformation.** We can benefit from very fine, down to the nanometre scale, precipitates that form at the α - γ interface as it travels into the austenite. We distinguish two forms of growth: *continuous* (**Slide 6**) and *interphase*. If you like you can think of the continuous growth of fibres in a similar way that you think of pearlite, the essential difference being that a carbide of a different element than Fe is being grown; and you might expect the same considerations to apply that lead to the Zener–Hillert theory. The mechanism of interphase precipitation is illustrated in cartoon form in **slide 8**. In contrast to continuous fibres interphase precipitates form in a periodic manner (it's best not to call this “discontinuous” as this has a special meaning, see **lecture 2, slide 10** and actually would apply to the “continuous growth of fibres”!) As the interface moves there are regular periods during which it does, and does not, nucleate and grow sheets of fine carbides within the interface; the carbides having one interface with the α and another with the γ . This leads to the development of a three phase orientation relation, as you will see in **lecture 7**, and this feature is a signature of interphase precipitation. As we have seen in **lecture 4** we expect at best partial equilibrium partitioning of substitutional elements as the α - γ interface sweeps into the austenite. So as the interface moves it is expected to accumulate substitutional alloying element so that as in the left hand cartoon in **slide 8** there exists a gradient of its concentration of composition c_{γ}^{α} at the interface and tailing off into the austenite. At this high concentration the carbide will simultaneously nucleate precipitates in a regular array in the plane of the interface. This precipitation serves to deplete the concentration of the transition metal at the interface and therefore for a while the interface will continue to move without any precipitation while the concentration builds up again to c_{γ}^{α} , upon which the process repeats. Actually it is expected that interphase precipitation is associated with the motion of steps at the interface as indicated in **slide 9**; in this case you'd expect that the spacing of the sheets will reflect the heights of the steps. **Slide 11** illustrates that interphase precipitation also happens during the growth of pearlite. Recall Lecture 3: as the α - γ area of

the pearlite–austenite interface moves into the austenite it behaves similarly to the α – γ interface in the growth of proeutectoid ferrite and hence if there are microalloy elements present they may well precipitate at the interphase in the same way. Indeed it is possible to find interphase precipitates within the cementite. **Slide 11** is a *dark field image* taken using a single reflection from the vanadium carbonitride. The authors find that all the precipitates are in contrast under these conditions and this is evidence that only one of the variants of the Baker–Nutting orientation relation are exhibited in the microstructure. This is a signature of interphase precipitation (see Lecture 7). **Slides 13–19** are taken from some recent steel design work at Sheffield University and King’s College London showing how vanadium carbide interphase precipitates are induced under an experimental heat treatment schedule. **Slide 20** shows sheet spacing as a function of isothermal transformation temperature.

4. **Low temperature precipitation in ferrite.** If the $\alpha \rightarrow \gamma$ transformation is at a low temperature isothermal treatment or at a high cooling rate then there is no time for precipitation during the transformation. If the resulting ferrite is supersaturated in microalloy elements then there is the possibility of age hardening; exactly as you are familiar from age hardening principles in aluminium alloys. In the same way, it is possible to obtain, under-aged, peak-aged and over-aged conditions. See **Slides 22–24**. Note the use of the Larson–Miller parameter in **Slides 23 and 24**; this is a means to combine time and temperature into a single number, such that some long time low temperature may equate to some other short time high temperature condition. It is used a lot in plotting and extrapolating creep data. The log is there because things that increase linearly in time, such as the extent of a reaction, usually depend exponentially on temperature through the Boltzmann factor. In **Slides 23 and 24** T is in Kelvin and t is in hours.

Further reading

- R. W. K. Honeycombe, “Steels: Microstructure and Properties,” Edward Arnold, 1st Edition, 1981
- A. T. Davenport and R. W. K. Honeycombe, *Proc. Roy. Soc. A*, **322**, 191 (1971)
- R. W. K. Honeycombe, *Met. Trans. A*, **7A**, 915 (1976)
- Special Issue of *Mat. Sci. Technol.*, **25**, issue 25, (2009)
- T. Epicier, D. Acevado and M. Perez, *Philosophical Magazine*, **8**, 31 (2008)
- P. Gong, E. J. Palmiere and W. M. Rainforth, *Acta Metall.*, **119**, 43 (2016)

Problems

- 6.1 Why is it necessary to hot-roll a microalloy steel in order to induce carbide precipitation in austenite?
- 6.2 How and why does the interphase precipitate size and sheet spacing depend on the transformation temperature?
- 6.3 Explain what is meant by the terms *under-aging*, *peak-aging* and *over-aging* in the context of age hardening of alloys. Under what conditions of composition and heat treatment would you expect to achieve age hardening in steels? How are the different mechanisms of particle hardening—cutting and bowing—reflected in the relative increases in yield strength and tensile strength?

Lecture 7

7-1 Martensite in Steel

Martensite in steel comes about through an athermal transformation, usually as a consequence of very rapid cooling, or *quenching*. The characteristics are well known: a hard phase consisting of body centred tetragonal iron, and possibly carbides and retained austenite, the new phase appearing in the microstructure as laths or plates the latter associated with surface tilting observed on polished surfaces (**slide 2**). There is a characteristic habit plane (referred to the γ -phase) and orientation relation, OR, (**slide 3** and see section 7-2) which can be observed in the electron microscope or by two surface measurements in X-ray diffraction. We separate steel martensite roughly into three groups (**slide 17**):

Low carbon martensite. Habit plane: $\{557\}_{\gamma}$, K-S OR. The habit plane is often reported as $\{111\}_{\gamma}$ which is 9.4° from $\{557\}_{\gamma}$. Found in steels with carbon up to 0.5wt%, and Fe-Ni-Mn alloys. Lath microstructure, showing a hierarchy of laths, blocks and packets within a prior austenite grain (**slide 21**).

Medium carbon martensite. Habit plane: $\{225\}_{\gamma}$, K-S OR. Microstructure of lenticular plates. Steels with 0.5–1.4wt% C. May occur in bursts. Up to 1wt% C may appear alongside lath martensite.

High carbon martensite. Habit plane: $\{259\}_{\gamma}$, N-W OR. wt% C > 1.4. Also plate microstructure with bursts (**Slides 27 and 28**).

7-2 Orientation relations in martensite

Always when considering the coexistence of two or more crystalline phases one is interested in both the *habit plane* and the *orientation relationship*. “Habit plane” refers to the orientation of the macroscopic plane that separates two phases. This only has meaning if the interface is flat and extensive, for example in a lenticular or lath shaped microstructure. “Orientation relationship” means the relationship that would exist between the phases’ two crystal lattices if they were allowed to interpenetrate in a thought experiment.

Three well-known orientation relationships in steels are,

Kurdjumov–Sachs (**K–S**)

$$\begin{aligned}(111)_{\gamma} &\parallel (101)_{\alpha} \\ [1\bar{1}0]_{\gamma} &\parallel [11\bar{1}]_{\alpha}\end{aligned}$$

Nishiyama–Wasserman (**N–W**)

$$\begin{aligned}(111)_{\gamma} &\parallel (110)_{\alpha} \\ [\bar{1}10]_{\gamma} &\parallel [001]_{\alpha} \\ [11\bar{2}]_{\gamma} &\parallel [\bar{1}10]_{\alpha}\end{aligned}$$

Greninger–Troiano (**G–T**)

$$(111)_\gamma \parallel (110)_\alpha$$

$$[\bar{1}2\ 17\ \bar{5}]_\gamma \parallel [\bar{1}7\ 17\ 7]_\alpha \text{ or } [\bar{1}2\bar{1}]_\gamma \text{ } 1^\circ \text{ away from } [1\bar{1}0]_\alpha$$

as you can see, close packed planes in each phase are parallel; in the case of K–S close packed directions are also parallel. **Slide 4** shows a projection of the atoms of fcc and bcc Fe onto their close packed planes. The two crystals are rotated about the normals of these planes into the **N–W OR**. Note that if the rotations denoted R^+ and R^- are zero then the **K–S OR** is obtained.

1. Many habit planes are observed, including planes on or near (111), (112), (225), (557), (259), (3 10 15) given as always in the crystal lattice system of the parent fcc austenite. The habit plane usually depends on composition but (225) and (259) may occur in the same specimens of many steel compositions: Fe–C, Fe–Ni–C, Fe–Cr–C and Fe–Mn–C. Some observed habit planes may be irrational but within less than a degree from one of the these.
2. The orientation relation may also be irrational. It is thought that the observed N–W orientation is such a case. For example, In Fe–0.8%C–22%Ni a habit plane between (3 10 15) and (9 22 33) is observed having an orientation relation of $(111)_\gamma$ about 1° from $(110)_\alpha$ and $[\bar{1}10]_\gamma$ about 2° from $[001]_\alpha$. In steels having compositions Fe–0.20%C–0.51%Mn–0.45%Si and Fe–0.42%C–0.52%Mn–0.48%Si martensite with a habit plane of (575) is observed with an orientation relation of $(111)_\gamma \parallel (011)_\alpha$ and $[\bar{1}01]_\gamma$ on average 3.1° from $[\bar{1}\bar{1}1]_\alpha$. The same crystallography is observed in Fe–20%Ni–5%Mn (except that the angle of 3.1° is measured to be 3.9°); this alloy has a lower M_s temperature so it is easier to obtain retained austenite to assist in the electron microscopy analysis of the crystallography.
3. Because of the cubic symmetry of the austenite and tetragonal symmetry of the martensite there is a number of *variants* of each habit plane and orientation relation. There are 24 variants of the K–S orientation and in (225) and (557) martensite these comprise 12 twin pairs (see **slide 21**). This is why lath martensite is said to form laths, blocks and packets (see **slide 20**, and **slide 14** in **lecture 3**). The laths within a packet all have the same variant of the habit plane, or have variants that are close together: for example (557) and (575) may appear in the same packet as their normals are just 16° apart. However these parallel laths may belong to different variants of the orientation relation. Those laths within a packet which are contiguous and belong to the same orientation are said to form a block. So the laths within a block are separated by a boundary that is not really a grain boundary as there is no misorientation between the two laths. The “boundary” is really then just a collection of dislocations arising from the lattice invariant deformation. At some points along the boundary the two laths are sometimes observed to be merged together. This is why it is likely to be *either* the block size *or* the packet size that enters into the Hall–Petch relation. Each prior austenite grain will be separated into individually nucleated packets so that the packet boundaries are high angle boundaries. In order to minimise the total shear strain energy, in each prior austenite grain there should be at least one packet from each of the habit plane variants. The block grain boundaries may be low or high angle grain boundaries.

4. Within a packet of (557) martensite there may be found a number of those variants of (557) that are close to one of the four $\{111\}$ variants of the habit plane; in that case the block structure may be understood in terms of the six variants of the K–S OR shown in **slide 21**. It has recently been suggested that each block actually comprises *two*, not *one* OR: the two being related by having the same “Bain axis”, that is, they derive from the compression of the same $[001]_\gamma$ direction in the Bain correspondence. Analysis based on an assumed (111) habit means that the laths in each packet are *approximately* parallel to (111) and hence the habit plane of (557) martensite may be observed to be (111). Hence you will read of (111) martensite but it is probably actually (557) martensite.

7–3 Orientation relations between carbides and ferrite

Since we are discussing orientation relations, we may as well include here descriptions of those between commonly occurring transition metal carbides and the matrix. As you will see, observations of the OR may be crucial in determining the mechanism of the precipitation reaction.

In the case of transition metal carbides in ferrite, bainite or martensite, the subscript “ γ ” is to be replaced by “ c ” for carbide, as in the following.

Baker–Nutting (**B–N**)

$$(001)_c \parallel (001)_\alpha$$

$$[100]_c \parallel [110]_\alpha$$

cube–cube is self evidently

$$(100)_c \parallel (100)_\alpha$$

$$[001]_c \parallel [001]_\alpha$$

assuming that this refers to a carbide belonging to a *cubic* crystal system.

The strongest evidence for interphase precipitation is that the resulting (cubic) carbides, for example, VC, V_4C_3 , NbC, TiC, TaC, are either all found to be a single variant, or are not found in a variant of the Baker–Nutting orientation at all which would be the case for carbide precipitated in the bulk of a ferrite grain, for example during tempering. Instead there is a three phase relation, namely K–S between α and γ , K–S between the cubic carbide and the α , and a cube–cube between the carbide and the γ phases. This points rather clearly to the carbide being precipitated at the moving α / γ interface. In the case of the $M_{23}C_6$ types of carbides, for instance $Cr_{23}C_6$ (see **slide 10**, lecture 6), the carbide is in K–S orientation with respect to ferrite and in a cube–cube relation with austenite so that the overall observed orientation relationship is

$$(111)_\gamma \parallel (1\bar{1}0)_\alpha \parallel (111)_{Cr_{23}C_6}$$

$$[\bar{1}10]_\gamma \parallel [\bar{1}11]_\alpha \parallel [\bar{1}10]_{Cr_{23}C_6}$$

This is as good a place as any to give you observed orientation relationships between iron carbide, Fe_3C , and ferrite. Note that the iron carbide in pearlite is the orthorhombic

cementite, or θ -Fe₃C. In the early stages of tempering and in nanostructured steels it is common to find the hexagonal ε -Fe₃C (see **lecture 8**).

Two orientation relations are commonly found in pearlite between cementite and ferrite, both often found in the same specimen. These are,

Pitsch–Petch

$$\begin{aligned} & (001)_\theta \parallel (5\bar{2}1)_\alpha \\ [100]_\theta & \text{ 2–3}^\circ \text{ away from } [13\bar{1}]_\alpha \\ [010]_\theta & \text{ 2–3}^\circ \text{ away from } [113]_\alpha \end{aligned}$$

Bagaryatski

$$\begin{aligned} & (001)_\theta \parallel (211)_\alpha \\ [100]_\theta & \parallel [0\bar{1}1]_\alpha \\ [010]_\theta & \parallel [1\bar{1}\bar{1}]_\alpha \end{aligned}$$

Measurement of the orientation relation between cementite and lower bainitic ferrite has fueled the debate about whether the cementite is precipitated *during* or *after* the formation of the bainite plate (see **lecture 5**). The fact that the orientation relationship is sometimes observed to be just one of the variants of the Bagaryatski relation, and that the cementite precipitates invariably have a habit plane that make an angle of 60° to the axis of the plate supports the argument that cementite precipitates *during* bainite reaction by interphase precipitation. On the other hand Bhadeshia and Edmonds found the orientation to be

$$\begin{aligned} & (011)_\theta \parallel (011)_\alpha \\ [1\bar{2}2]_\theta & \parallel [100]_\alpha \end{aligned}$$

in a silicon steel, and this is incompatible with there being the expected θ - γ - α three phase relation as discussed above in the context of interphase precipitation of the carbides of microalloying elements. I think that I incline to follow Bhadeshia and believe that in lower bainite the carbide is precipitated *after* the displacive transformation from austenite to ferrite. See **lecture 5**.

ε -Fe₃C is essentially hcp iron with carbon in the octahedral interstices. It is found in the so called Jack orientation relation,

$$\begin{aligned} & (0001)_\varepsilon \parallel (011)_\alpha \\ (10\bar{1}0)_\varepsilon & \parallel (2\bar{1}1)_\alpha \end{aligned}$$

Further reading

H. K. D. H. Bhadeshia and R. W. K. Honeycombe, "Steels: Microstructure and Properties," Elsevier, 3rd Edition, 2006

<https://www.youtube.com/watch?v=FffY381eMhU>

<https://www.youtube.com/watch?v=S-5ZMhE7Iak>

B. P. J. Sandvik and C. M. Wayman, *Metallography*, **16**, 199 (1983)

H. Kitahara, R. Ueji, N. Tsuji and Y. Minamino, *Acta Metall.*, **54**, 1279 (2006)

C. C. Kinney, K. R. Pytlewski, A. G. Khachaturyan and J. W. Morris Jr., *Acta Metall.*, **69**, 372 (2014)

L. Qi, A. G. Khachaturyan and J. W. Morris Jr., *Acta Metall.*, **76**, 23 (2014)

X. Ma and R. C. Pond, *J. Nuclear Materials*, **361**, 313 (2007)

H. K. D. H. Bhadeshia and D. V. Edmonds, *Met. Trans. A*, **10A**, 895 (1979)

H. K. D. H. Bhadeshia, *Acta Metall.*, **28**, 1103 (1980)

Problems

- 7.1 Look back at slide 14, lecture 1; and explain using some detail the trends that are observed. Why is martensite the strongest phase in these HSLA steels?
- 7.2 Why is it necessary that the martensitic shape change is an invariant line strain? Explain why this condition is in fact more stringent, requiring the shape change to be an invariant plane strain. In your answer state what are invariant line and invariant plane deformations. How is it possible that the Bain correspondence can become an invariant plane strain?
- 7.3 Why are both habit planes and orientation relations in martensite usually irrational? In your answer state what is meant by "irrational."
- 7.4 By reference to the Bain correspondence explain why carbon steel martensite is always tetragonal.
- 7.5 What is meant by an athermal phase transformation? How is such a transformation recognised in a TTT diagram? Is steel martensite always athermal? How is burst martensite distinguished in both transformation kinetics and microstructure?
- 7.6 In the case of lath martensite, why is it that the lath width does not really control the Hall-Petch slope?
- 7.7 Look at **slide 21**. Can you identify the pair of variants that share a "Bain axis"? Can you identify pairs that are twin related?
- 7.7 Look at **slide 22**. On the right a large packet is coloured orange. The same packet on the left has the laths coloured according to which of the six variants of the OR they have. Can you see why it is proposed that each block is actually made up of pairs of variants sharing a "Bain axis"? The colours in the left hand figure correspond to those in **slide 21**.

Lecture 8

*So, grasping hard the stake pointed with fire,
 We twirl'd it in his eye; the bubbling blood
 Boil'd round about the brand; his pupil sent
 A scalding vapour forth that sing'd his brow,
 And all his eye-roots crackled in the flame.
 As when the smith an hatchet or a large axe
 Tempr'ing with skill, plunges the hissing blade
 Deep in cold water, (whence the strength of steel)
 So hiss'd his eye around the olive-wood.*

The Odyssey of Homer
 Translated by William Cowper

Like most translators Cowper has translated Homer's original word $\beta\alpha\pi\tau\omega$ meaning "dip" (as in "baptize") as "temper." In fact the Poet is describing quenching, not tempering. We will now cover both these in this lecture.

Hardenability is described as the ability of a steel to form martensite upon quenching. This is a very qualitative definition, so it is necessary to develop quantitative measures. Generally this involves heating a standard size and shape of specimen to the fully austenitic state and then after quenching, assessing by metallography or by hardness measurement how far from the surface the steel has transformed to martensite rather than a softer product such as ferrite and pearlite. We should not use TTT diagrams except to discuss isothermal transformation, nevertheless **slide 2** serves to point out that the rate of cooling needs to be fast enough to avoid any "noses" in the TTT diagram, and that this condition may be met near the surface but not at the centre of the piece, since there the cooling rate will be less. If the specimen is in the form of a bar then the depth of hardening will of course depend on the diameter of the bar as indicated in **slide 3**.

Think about what happens when the hot metal is dropped into a quenching medium, be it water, brine, oil or a polymer quench. We distinguish three stages.

1. **Vapour blanket stage.** When the steel meets the quench medium a blanket of vapour is immediately created isolating the piece from the medium so that heat loss is by radiation and rather slow and is governed by the *emissivity* of the steel.
2. **Nucleate boiling.** The vapour blanket collapses and the liquid makes contact with the piece and boils. The onset of this stage can be quickened by using a high boiling point medium, for example a salt solution. This is the stage of the highest cooling rate, but it is relatively short.
3. **Convective cooling** Once the medium stops boiling the system settles down into convective cooling and the cooling rate is governed by the heat transfer coefficient. This stage is the longest and so dominates the final microstructure.

Slide 5 shows these stages in cartoon form by tracking the temperature (in red) and cooling rate (in blue). T_{vp} and T_{cp} are the temperatures at the onset of the vapour and convection phases. You see that the first two are over after about ten seconds and the rate of cooling for the largest part of the quench is dominated by the convective phase. Therefore we focus now on that part of the quench in an attempt to extract a quantitative measure of what is called the *quench severity*.

Recall the theory of heat transfer. The transfer of heat by *conduction*, that is, within the piece, is governed by Fourier's law for the heat flux,

$$q = -k \frac{\partial T}{\partial x} \quad [\text{J s}^{-1} \text{ m}^{-2}]$$

in which k is the *thermal conductivity*; and the heat conduction equation for the temperature variation with time,

$$\dot{T} \equiv \frac{\partial T}{\partial t} = \kappa \frac{\partial^2 T}{\partial x^2}$$

in which κ is the *thermal diffusivity*, both given in one dimension for simplicity. On the other hand the rate of cooling of a body by loss of heat to the outside is approximately described by Newton's law of cooling,

$$q = h \Delta T = h \times (\text{temperature of body} - \text{temperature of surroundings})$$

in which h is the *heat transfer coefficient*. Note that in Fourier's law the proportionality coefficient between the heat flux q and the (negative) temperature gradient is the *thermal conductivity* having units of $[\text{J s}^{-1} \text{ m}^{-1} \text{ K}^{-1}]$. On the other hand the coefficient in the heat conduction equation is the *thermal diffusivity*, which is the ratio of the thermal conductivity and the heat capacity per unit volume. This then has the units of a conventional transport coefficient, $[\text{m}^2 \text{ s}^{-1}]$, as does the diffusivity in Fick's second law and the kinematic viscosity which is the viscosity in $[\text{N s}^{-1} \text{ m}^{-2}]$ divided by the mass density.

The coefficient that enters Newton's law of cooling is the convective heat transfer coefficient h . This is the heat flux, (watts per square metre) crossing the surface of the metal into the medium, divided by difference in temperature ΔT between the surface and the medium. It therefore has units of $[\text{J m}^{-2} \text{ K}^{-1} \text{ s}^{-1}]$. For the case of a cylindrical bar,

$$h = -\frac{\rho V c_p \dot{T}}{A \Delta T}$$

where ρ is the density of the steel, c_p is its mass specific heat and V and A are volume and surface area. $-\dot{T}$ is the cooling rate.

The conditions during a quench are determined *both* by the rate of conduction from the inside to the surface of the piece *and* by the rate of heat transfer by convection into the quench medium. You are aware that transport phenomena problems (especially involving two competing processes) are greatly clarified by the use of dimensionless

quantities, for example the Reynolds number in viscosity problems which is the ratio of inertial to viscous forces. Where there are both conduction and convection we are interested in the ratio of the heat transfer to the thermal conductivity. To make up a dimensionless number we need a factor L of dimension length. The *Biot number* is[†]

$$\text{Bi} = \frac{hL}{k}$$

(Do not confuse this with the Nusselt number which has the same formula but for which the conduction takes place in the fluid not the solid and so k is the thermal conductivity of the *fluid*). In our case a suitable characteristic length will be half the volume of the bar divided by its surface area: $V/A = 2L$, so that L is roughly a quarter of the radius of the bar.

Now I can define for you the so called Grossman quench severity, $H(T)$, which is a function of temperature. By convention this is defined as the convective heat transfer coefficient divided by twice the thermal conductivity of the steel. It has units of $[\text{m}^{-1}]$,

$$\begin{aligned} H(T) &= \frac{h}{2k} \\ &= \text{Bi} \frac{A}{V} \end{aligned}$$

Slides 7 and 8 show data on thermal conductivity and diffusivity in some steels. (1Btu \approx 1kJ—do you know what Btu stands for?) **Slide 9** shows how the H-value varies at the midway and the centre of a bar during a quench as a consequence of its temperature dependence. The table in **slide 10** indicates how we can associate the quench severity with the conditions and the medium of the quench (I assume that the values are in $[\text{inch}^{-1}]$ as in **slide 9**).

[†] Let me quote to you from the [wikipedia](#) article on the Biot number. “The physical significance of Biot number can be understood by imagining the heat flow from a small hot metal sphere suddenly immersed in a pool, to the surrounding fluid. The heat flow experiences two resistances: the first within the solid metal (which is influenced by both the size and composition of the sphere), and the second at the surface of the sphere. If the thermal resistance of the fluid/sphere interface exceeds that thermal resistance offered by the interior of the metal sphere, the Biot number will be less than one. For systems where it is much less than one, the interior of the sphere may be presumed always to have the same temperature, although this temperature may be changing, as heat passes into the sphere from the surface. The equation to describe this change in (relatively uniform) temperature inside the object, is simple exponential one described in Newton’s law of cooling. In contrast, the metal sphere may be large, causing the characteristic length to increase to the point that the Biot number is larger than one. Now, thermal gradients within the sphere become important, even though the sphere material is a good conductor. Equivalently, if the sphere is made of a thermally insulating (poorly conductive) material, such as wood or styrofoam, the interior resistance to heat flow will exceed that of the fluid/sphere boundary, even with a much smaller sphere. In this case, again, the Biot number will be greater than one.”

Continuing our theme of trying to quantify the hardenability, refer back now to **slide 3**. For a bar of a particular diameter, D , the microstructure will probably be fully martensitic on the outside and the fraction of martensite will become less, moving inwards, and there may be no martensite at all at the centre. Let us imagine performing this experiment using identical soaking and quenching conditions but using bars of varying diameter. If we section the bar and make a metallographic examination of each bar we can determine the diameter of that bar which has a microstructure comprising exactly 50% martensite at its centre. We will call this the *critical diameter*, D_0 . This is *still* not a quantitative measure of hardenability that we can convey to other engineers because of course the critical diameter that we get will depend on the severity of quench. So why not invent a quantity called the *ideal diameter*, D_i , that is the critical diameter we would get if we could use an infinite quench severity? Given that after much tedious labour, machining, soaking, quenching, sectioning, polishing and examining bars of different diameters we have a critical diameter for the quench we are using, how can we convert this into an ideal diameter so that we have a repeatable index of the hardenability of our steel? The answer is that we use the table and chart in **slides 10** and **11**. First we estimate the severity of quench in our experiment, then reading off from the chart we choose the line appropriate to our quench and find the ideal diameter corresponding to our critical diameter (again, I'm assuming that the quench severity lines marked off in the chart on **slide 11** are in units of inverse inches and that D and D_i are in centimetres). It is clear that the ideal diameter is larger than the critical diameter because if the quench were infinitely severe then a larger diameter bar will still result in having 50% martensite at its centre.

The Jominy test (below) does not result in a single measure of hardenability although the results contain a wealth of data. On the other hand the Grossman ideal diameter is a measure of hardenability that is independent of the method of quench and hence properly regarded as a materials parameter. For example the effect of different alloy elements may be tested to determine which imparts the greater hardenability. As we have already seen earlier these include molybdenum and boron.

The two principal factors controlling hardenability are prior austenite *grain size* and *composition*. There is a procedure to predict hardenability for a given steel. First use a chart like **slide 12** to read off the *base hardenability*, $D_{i,crit}$, as a function of carbon concentration and grain size. Then there are multiplicative factors to take into account alloying elements using this empirical relation,

$$D_i = D_{i,crit} \times 3.28(\text{wt}\% \text{Mo}) \\ \times 2.21(\text{wt}\% \text{Mn}) \times 2.13(\text{wt}\% \text{Cr}) \times 1.47(\text{wt}\% \text{Ni}) \times 1.40(\text{wt}\% \text{Si})$$

Slide 13 shows these individual *hardenability factors*. I don't know why they are not straight lines as required by the empirical formula. The effect of boron is powerful and a further multiplying factor is applied for this as indicated in **slides 15–18**.

It is important for the engineer not to overdo hardenability. For example steels are regarded as not weldable if their "carbon equivalent" exceeds about 0.4wt%. This is because a hard and untempered martensite may be produced in the heat affected zone

that will lead to cracking. The C.E. can be calculated using a formula such as this.

$$\text{Carbon Equivalent} = \text{wt}\% \text{ C} + \frac{\text{wt}\% \text{ Mn}}{16} + \frac{\text{wt}\% \text{ Si}}{43} + \frac{\text{wt}\% (\text{Ni} + \text{Cr})}{28} + \frac{\text{wt}\% \text{ Mo}}{22}$$

The Grossman hardenability is well worth studying because it's easy to appreciate the metallurgical and engineering principles leading to the definition of a materials property that can be communicated between practitioners and steel makers. However the experiments are too time consuming to make this a routine practice for alloy designers and metals testing laboratories. As an alternative it is more common to make a Jominy end quench test. A bar of standard dimensions is annealed and placed in a rig where it is subjected to a jet of water impinging at one end of the bar. The hardness is then measured at intervals along the bar and the surface hardness is plotted as a function of distance from the quenched end. The dimensions are given in **slide 19** and some typical data plotted in **slide 20**. To make contact with the Grossman test there are standard curves that can be produced (**slide 21**) which can be used to relate hardness to the percentage of martensite for a given steel. To complete the connection between the two we need to know how the Jominy quench using a jet of water from one end of a bar relates to a quench in which the bar is fully immersed in a quench medium at a certain quench severity. Again, there are standard curves that can be consulted, such as **slide 22**. The rate of cooling at a chosen distance from the quenched end in the Jominy test is the same as the rate of cooling at the centre of a Grossman bar given by the curve appropriate to the quench severity of the Grossman quench. That is, to find the diameter of bar that would have the same cooling rate at its centre as the cooling rate a certain distance along the Jominy bar, just select the distance along the x -axis and using the curve for the appropriate quench severity in the Grossman test, read off the diameter of bar on the y -axis whose centre will experience the same cooling rate as that part of the Jominy bar.

As you know martensite is generally speaking too hard to be of practical use. Therefore it is tempered after quenching to bring about a balance of strength and toughness by allowing some of the carbon to diffuse out of the supersaturated martensite and produce isothermal products such as bainite or ferrite, containing precipitated iron carbides. Tempering *temperature* is generally more important than tempering *time* in bringing about the desired microstructure. **Slide 24** shows the effects of tempering temperature on a number of mechanical properties of a quenched and tempered steel.

Four stages in tempering have been identified and I will now describe these. They are summarised in **slide 25**.

Stage 1

Carbon diffuses from room temperature up to 250°C, so for steels with more than 0.3wt% C, martensite is unstable in this temperature range and ϵ -Fe₃C precipitates (**slide 26**). This is hexagonal close packed iron, having C atoms occupying up to 1/3 of the octahedral interstices lying in between the close packed planes. The orientation

relation with the martensite is as follows (see **lecture 7**).

$$\begin{aligned}(101)_{\alpha'} &\parallel (10\bar{1}1)_{\varepsilon} \\ (011)_{\alpha'} &\parallel (0001)_{\varepsilon} \\ [11\bar{1}]_{\alpha'} &\parallel [1\bar{2}10]_{\varepsilon}\end{aligned}$$

These are nearly coherent precipitates, and are likely to increase hardness by a particle cutting mechanism, see **slide 4, lecture 1**. Some ε -Fe₃C precipitates are shown in **Slide 26**).

Stage 2

Principally this is transformation of retained austenite in the temperature range 230–300°C. It is supposed that the transformation products are bainite and cementite.

Stage 3

This stage is characterised by the first appearance of cementite also known as θ -Fe₃C, and by the loss of tetragonality of the martensite. The orthorhombic cementite forms in an orientation relation with the martensite as follows. This is essentially the Bagaryatski relation of **lecture 7** (notes page 3).

$$\begin{aligned}(211)_{\alpha'} &\parallel (001)_{\theta} \\ [01\bar{1}]_{\alpha'} &\parallel [100]_{\theta} \\ [\bar{1}11]_{\alpha'} &\parallel [010]_{\theta}\end{aligned}$$

This reaction may begin at 100°C, and fully develop at 300°C. Cementite particles are up to 200 nm long and ~15 nm thick. The cementite probably nucleates at the ε -Fe₃C interfaces with martensite (**slide 26**). Cementite eventually consumes the ε -Fe₃C. Cementite may also nucleate on twins which occur in higher carbon martensite, which then grows into colonies of θ -Fe₃C laths (**Slide 27**) having habit planes of $\{112\}_{\alpha'}$ type. Cementite will also nucleate at prior austenite grain boundaries (**Slide 28**) and at martensite lath boundaries. The nuclei grow into thin films which subsequently spheroidise. At the end of stage three the martensite is essentially ferrite, all tetragonality being lost.

Stage 4

This is a stage of cementite coarsening between 300°C and 400°C, followed by spheroidisation at up to 700°C. The resulting microstructure contains equiaxed grains of ferrite and coarse spheroidal cementite (**Slide 29**)

Martensite lath boundaries may remain stable up to about 600°C, but there are rearrangements of the lath boundaries and dislocations within the laths in the range 350–600°C, resulting in a reduced dislocation density and reduction in hardness. This is essentially static recovery.

Slide 30 summarises the hardness reduction in the different stages described for martensites having various carbon contents. The anomalous *increase* in hardness in the initial stages of tempering 0.18% C steel may be attributed to hardening by coherent ε -Fe₃C particles.

Further reading

https://en.wikipedia.org/wiki/Thermal_conduction

R. W. K. Honeycombe, "Steels: Microstructure and Properties," Edward Arnold, 1st Edition, 1981

W. C. Leslie, "Physical Metallurgy of Steels," McGraw-Hill, 1981

<https://www.youtube.com/watch?v=qW0aUbtWtVM> is a film of the Jominy end quench test.

Chen Zhu, Alfred Cerezo and George D. W. Smith, *Ultramicroscopy*, **109**, 545 (2009)

Problems

- 8.1 What is meant by the "hardenability" of steel? What is meant by "ideal critical diameter"?
- 8.2 Describe the Jominy end quench test used to measure the hardenability of a steel.
- 8.3 State what are the two principal variables that influence hardenability of steel.
- 8.4 Give an explanation for why boron in parts-per-million concentrations is able to improve hardenability. Why do larger amounts of boron have no further influence on hardenability?
- 8.5 Give an example of a substitutional impurity element that can be used to improve hardenability. Explain the physical origin of the effect produced.
- 8.6 What is meant by "tempering"? Why is it normally the practice to temper martensite?
- 8.7 Describe the four principal stages in the tempering of martensite, including for each stage the temperature range and the resulting microstructure.